**Sitae Kim**
Professor
Mem. ASME
Department of Mechanical Engineering,
Korea Air Force Academy,
Cheongju 28187, South Korea
e-mail: sitaekim@outlook.com

**Dongil Shin**
Department of Mechanical Engineering,
Texas A&M University,
College Station, TX 77840
e-mail: davshin@tamu.edu

**Alan B. Palazzolo**[1]
Professor
Fellow ASME
Department of Mechanical Engineering,
Texas A&M University,
College Station, TX 77840
e-mail: a-palazzolo@tamu.edu

# A Review of Journal Bearing Induced Nonlinear Rotordynamic Vibrations

*Nonlinear elements found in fluid film journal bearings and their surrounding structures are known to induce sub- and super-synchronous, chaos and thermally induced instability responses in rotor-bearing systems. The current review summarizes the literature on journal bearing induced nonlinear, rotordynamic forces, and responses. Nonlinear, thermo-elasto-hydrodynamic (TEHD) aspects of journal bearings has become increasingly important in high-performance turbomachines. These have significant influence on bearing dynamic performance and thermally induced, rotordynamic instability problems. Techniques for developing TEHD bearing models are discussed in the second section. Nonlinear solution methodology, including bifurcation determination and time and frequency domain methods such as harmonic balance, shooting and continuation, etc., is presented in the third section. Numerical tools to determine nonlinear vibration responses, including chaos, along with examples of bearing induced nonlinear vibrations are presented in the fourth and fifth sections, respectively.* [DOI: 10.1115/1.4049789]

*Keywords: bearing design and technology, bearings, fluid film lubrication, friction, hydrodynamic lubrication, thermoelastohydrodynamic lubrication*

## 1 Introduction

Fluid film journal bearings are ubiquitous among the power, petrochemical, and process industries as a result of superior load capacity, high-speed operation, long life, high reliability, etc. This holds, in spite of their physical complexity and potential to contribute significant nonlinear (NL) forces to the rotating assembly system. Fluid film bearing related characteristics such as self-excited oscillations [1–4], thermoelastic expansion [5–8], and fluid inertia [9,10] are known to induce nonlinear response states of the rotor system such as sub-synchronous, quasiperiodic, aperiodic, and even chaotic motions. Many researchers have contributed to this work in terms of novel theoretical and computational methods, along with experimentation. There has been a vast literature representing fluid film bearings in a linear form, i.e., stiffness, damping, and inertia dynamic coefficients [11]. System response characteristics such as natural frequencies, critical speeds, mode shapes, and log decrements are obtainable using the bearing dynamic coefficients (BDCs) along with the rotor structural model. In addition, small motion imbalance response can be predicted for response magnitudes smaller than the limits for the validity of the BDC force representation. The imbalance response distribution is unique (single valued) at a given speed and for a given imbalance distribution. The responses occur at the rotor speed frequency, so are referred to as synchronous responses. The validity of this result is limited by the approximation of the bearing forces being linear functions of journal displacement, velocity, and accelerations. In fact, the forces are nonlinear NL functions of these variables which may produce responses that radically differ from the linear system responses. Imbalance responses can then become multivalued (coexisting solutions) depending on initial conditions, sub or superharmonic, quasiperiodic, or chaotic. Linear system stability analysis utilizes eigenvalues and log decrements to indicate whether a given equilibrium state is stable or unstable for small perturbation of states in the neighborhood of the equilibrium state. Linear system stability analysis predicts an infinite response as time goes to infinity if the equilibrium state is unstable (negative log decrement, positive real part of eigenvalue). In actuality, responses remain finite in a bounded "limit cycle" (LC) in state space, which may be one of multiple coexisting limit cycles, as the nonlinear part of the bearing's force dominates with increasing amplitudes. Adding to the complexity of the NL response, coexisting imbalance and LC responses may appear or disappear as some system parameter such as speed or imbalance level is varied. This gives rise to a wide array or bifurcation behaviors, the most familiar of which is a "jump" bifurcation where the disappearance of an equilibrium state forces the system to "jump" to a remaining coexisting equilibrium state. Note that the term equilibrium state may refer to an orbital motion as well to a fixed point.

A popular approach to simulate nonlinear systems is to use brute force transient numerical integration (TNI), commonly with some form of Runge–Kutta method. The integration begins with a user selected state of initial values and proceeds until a periodic state is reached or until the system is judged to be aperiodic or chaotic. The nonlinear bearing forces are state dependent and are updated every predetermined number of integration time-steps, i.e., every time-step, every 2 time-steps, etc. The forces are evaluated from the instantaneous state variables using functional forms, look up tables or from independent codes that solve for bearing forces by integrating pressures that are obtained from the solution of Reynolds or Navier–Stokes equations. The transient nonlinear integration to steady-state (TNISS) method is easy to use and powerful to capture NL characteristics by providing journal orbits, frequency components, bifurcation diagrams, Poincaré sections, Lyapunov exponents (LEs), etc. Therefore, many publications including Adiletta et al. [12], Holt et al. [13], Tian et al. [14,15], and Schweizer [3] and many others utilize this approach.

The weakness of the TNISS method is its inability to locate multiple coexisting solutions in a computationally efficient manner. For instance, if an $n$ state system had the expected range of each initial condition state divided into $m$ points, $n^m$ separate numerical integration (NI) solutions to steady state would be needed to search this initial condition grid for multiple coexisting, steady-state solutions. A 20 degrees-of-freedom (DOF) rotor model has $n = 40$, each of which for the sake of illustration is divided into $m = 8$ initial

[1]Corresponding author.

Contributed by the Tribology Division of ASME for publication in the Journal of Tribology. Manuscript received July 2, 2020; final manuscript received January 6, 2021; published online February 12, 2021. Assoc. Editor: Patrick S. Keogh.

  

condition points. Then, $40^8 = 6.5 \times 10^{12}$ TNISS would be required to cover all points on the initial condition grid. Even in this case, $m$ may not be large enough to identify the coexisting equilibrium states. The importance of determining the coexisting solutions can in some instances not be overstated. The reason is that a system could "jump" from a benign solution to a potentially destructive solution in response to an impact (bump) or other upset condition. In addition, TNISS will never converge to an unstable "repellor" coexisting solution. This may appear irrelevant however repellors typically provide boundaries for domains of attraction for stable solutions.

In contrast, a direct search algorithms (DSA) approach uses an algorithm-directed search to determine all possible coexistent response states. DSA can be roughly categorized into two general approaches: the assumed periodic approximate form (APAF) and the assumed periodic numerically integrated form (APNIF). The harmonic balance method (HBM) is an APAF approach and was applied to find synchronous and sub-synchronous response state of rotor systems with stator rubs and squeeze film dampers, respectively, in Refs. [16–19]. HBM can be combined with arc-length continuation to extend solution branches over varying system parameters in a rotor/stator contact problem, as in Ref. [20]. The trigonometric collocation method (TCM) is a second APAF approach that was utilized along with component mode synthesis (CMS) to calculate periodic responses of a multi-disk rotor system with a squeeze film damper in Refs. [21,22]. The APAF approach substitutes an assumed response and NL force, expressed in terms of a truncated series of sinusoidal harmonics, into the governing, nonlinear differential equations. The results, after combining like terms and enforcing linear independence, are a set of coupled nonlinear algebraic equations, with the same or more equations than unknowns. This approach is very effective in obtaining approximate forms for the coexisting solutions; however, it may become cumbersome in cases where the nonlinear forces have highly complicated forms or can only be expressed numerically. Determining the stability of the solutions may also become very challenging and require applying Floquet theory to sets of coupled, linear differential equations with periodically varying coefficient expressions.

The most common form of the APNIF approach is the shooting method, which is a numerical approach to solve two-point boundary value problems, and has been used to predict response states of nonlinear rotor systems. The objective of the shooting approach is to iteratively determine periodic solutions, resulting from periodic excitations or from limit cycle motions, by enforcing the condition that the state vector has the same value both at the beginning and at the end of a period of oscillation. Sundararajan and Noah developed a nonautonomous shooting approach with arc-length continuation and CMS to apply to flexible rotor systems with nonlinear squeeze film dampers and journal bearings [23,24]. An added benefit of the shooting method is that the eigenvalues of the shooting method's Jacobian matrix, corresponding to a converged periodic solution, directly provide a means to determine the stability of the solution, namely, if any eigenvalue magnitude exceeds 1, the solution is a repellor (unstable). Table 1 summarizes the different solution methods and related research examples.

Considerable experimental work has been performed related to nonlinear bearing forces and response. Tests have been reported on a variety of journal bearings widely used in industry, including plain journal bearings (PJBs), multi-pad tilting pad journal bearings (TPJBs), and floating ring bearings (FRBs). An early example was the oil whip/whirl experiments conducted by Newkirk and Taylor [25] in 1925. More recent publications involve more sophisticated experiments and corresponding simulations. Monmousseau et al. [26] performed experiments on the transient temperature distribution of a four pad TPJB during start-up, utilizing a thermo-elasto-hydrodynamic model for comparison. Forty thermocouples were installed on a journal and bearing to measure their temperature distributions, including the oil feed temperature. The measurements showed a rapid increase of pad temperature during the first 60 s and then a relatively slow increase after 120 s of operation.

Comparison with a prediction model showed reasonable agreement especially when the thermoelastic effect of pads was included in the simulations. Monmousseau et al. [38] conducted experimental work to validate their bearing seizure prediction model. Two start-up times of duration 3.5 s and 4.5 s were used, and the temperatures on the internal pad surface were measured with static loads of 0 N and 10,000 N. The comparison with the prediction results showed good agreement in both transient and steady-state tests. Kucinschi and Fillon [39] conducted an experimental study on the transient thermal characteristics in a plain journal bearing. The measured data revealed that an operating time of about 600 s was required to reach thermal steady-state conditions. The bearing temperatures increased with bearing load due to reduced axial oil flow. Table 2 presents some notable bearing experimental work in the literature.

The Morton effect (ME) is a thermally induced instability problem, which is typically observed in the rotor with overhung masses and supported by fluid film bearings. The large synchronous bearing whirl orbits resulting from the ME produce NL forces. Considerable effort has been devoted to accurately predict the ME for several decades. De Jongh and Morton [41] constructed a simplified rotor model to simulate the ME instability in original machines. The overhung mass was installed only at a non-drive end, and four temperature sensors were placed on 1.3 mm below the journal surface. From the test, they identified the ME instability which is characterized by spiral synchronous component vibrations, and high journal temperature differential, measured to be approximately 10 °C at 11.2 krpm. Balbahadur [42] measured a large vibration near the third critical speed (8 krpm), which could not be suppressed with balancing. Vibration amplitude hysteresis was observed during run-up and run-down operations, consistent with known ME symptoms. Journal temperature differential was not measured in the experiment. Panara et al. [43] built a ME testing rig to verify their simplified ME prediction method. Eight temperature sensors were installed on the journal circumference to measure the journal

**Table 1 Comparisons of different solution methods**

| | Transient numerical integrations | Harmonic balance method | Trigonometric collocation method | Hopf bifurcation theory | Shooting method |
|---|---|---|---|---|---|
| Categories | Integration method | Approximate method | Approximate method | Approximate method | Approximate method |
| Route to orbital steady states | Transient, initial value problem | Direct, algebraic problem | Direct, algebraic problem | Direct, boundary value problem | Direct, boundary value problem |
| Domain | Time | Frequency | Time and frequency | Time | Time |
| Multiple coexistent solutions | No | Yes | Yes | Yes | Yes |
| Research examples | Adiletta et al. [12], Suh and Palazzolo [7,8] | Groll and Ewins [20], Zhao and Hahn [27] | Nataraj and Nelson [21], Chinta and Palazzolo [28] | Wang and Khonsari [29–33], Boyaci et al. [34] | Sundararajan and Noah [23,24], Kim and Palazzolo [35–37] |

Table 2 Comparisons of experimental works in nonlinear bearing

| Source of nonlinearity | Hydrodynamic instability | Thermally induced instability | Disc mass unbalance | Rub, friction |
|---|---|---|---|---|
| Types of nonlinear response | Oil whirl; oil whip | Morton phenomena, divergence | Chaos; aperiodic response | Sub-synchronous, quasiperiodic, aperiodic |
| Research groups | Newkirk and Taylor [25], Deepak and Noah [40] | De Jongh and Morton [41], Balbahadur [42], Panara et al. [43], Tong and Palazzolo [44], Plantegenet et al. [45,46] | Adiletta et al. [12], Mondy [47] | Lu et al. [48], Chu and Lu [49] |
| Bearing types | Plain journal bearing | Plain journal bearing, tilting pad journal bearing | Plain journal bearing | Tilting pad journal bearing |

temperature differential. Their work showed that the speed range of the ME instability is related to the shift of the overhung critical speed. Tong and Palazzolo [44] conducted an experiment to compare with their ME prediction method. They spun a shaft with an intentionally eccentric journal to impose a 0.003 in. circular, synchronous whirl orbit in the TPJB. The journal temperature distribution was measured with 20 resistance temperature detectors (RTDs) embedded near the journal surface and routed through a slip ring. The results showed a relatively high journal temperature differential of 5 °C at 5500 rpm, and the results from their ME prediction approach provided better prediction accuracy compared with simplified algorithms. Plantegenet et al. [45,46] recently presented a series of experiments for ME utilizing PJB and flexure pivot TPJB. Thermocouples were installed in the journals and bearings to measure temperatures. They revealed that rig run-up time could significantly influence the thermally induced rotordynamic instability.

Thermo-elasto-hydrodynamic interaction is a source of nonlinearity in a rotordynamic system. Other factors that contribute to nonlinearity are listed below.

**1.1 Porous Pad.** The nonlinear behavior of the porous tilting pad journal bearing (PTPJB) is discussed in Ref. [50]. Unlike a standard TPJB, the PTJB is provided with externally pressurized gas to the clearance between the journal and pads, and therefore benefits from both hydrostatic and hydrodynamic actions. Both the TPJB and PTPJB cases were numerically simulated, and it was verified that the PTPJB improves the system stability by suppressing subsynchronous vibration, typically observed when the TPJB operates above critical speeds.

**1.2 Surface Roughness.** The surfaces of the journal and bearing are inherently rough due to the limitations of the manufacturing techniques, and this aspect affects the dynamic response of a system. Ramesh and Majumdar [51] examined the effect of the surface roughness and its pattern on the stability of a rigid rotor. The stability of the rotor varied with different roughness patterns and ratios on both journal and bearing surfaces, and the degree of the variation depended on the bearing *L/D* ratio. Turaga et al. [52] studied the surface roughness effect on the transient stability of a rotor, modeled with a finite-length journal bearing model. Fourth-order Runge–Kutta method was used to obtain the numerical solutions, and the results showed that the stability is enhanced with transverse roughness patterns and reduced with a longitudinal roughness pattern. Lin [53,54] used Hopf bifurcation theory (HBT) to obtain the weakly nonlinear bifurcation responses of a short journal bearing with transverse and longitudinal rough surfaces. Their results show that the effects of longitudinal roughness increase the stability region and reduce the size of subcritical and supercritical limit cycles. The effect of transverse surface roughness was reported to have the opposite effects.

**1.3 Pivot Design.** Suh and Palazzolo [7,8] conducted a Morton effect simulation with different pivot stiffness of a TPJB. Tong and Palazzolo [55,56] investigated the effect of the TPJB's pivot stiffness Morton effect analysis with a double overhung rotor and verified that pivot flexibility plays a significant role in accurately predicting the vibration responses caused by the Morton effect.

**1.4 Actively Lubricated Tilting Pad Journal Bearing.** Haugaard and Santo [57] applied a transient EHD analysis to an actively lubricated TPJB application. A flexible pad was modeled with a finite element method and integrated into a TPJB dynamics model with a pseudo modal reduction technique. Oil is actively injected through orifices located on the pad to influence static eccentricity, dynamic coefficients, and mitigation of nonlinear responses.

**1.5 Non-Newtonian Journal Bearing.** Zhang et al. [58], Zhang and Cheng [59], and Zhang [60] performed trainset thermohydrodynamic (THD) and TEHD on a dynamically loaded non-Newtonian journal bearing, operating in a mixed lubrication regime. The authors utilize a nonlinear shear stress-velocity gradient power law. Their model includes a one-dimensional surface roughness model applied in the longitudinal and transverse directions. It was found that the surface roughness of a journal and a bushing increases an oil temperature oscillation cycle and also decreases the average heat absorption cycle into the shaft [58]. It was also verified that the temperature distribution in a bearing is quite sensitive to the asperity contact level [60].

**1.6 Pad Rubbing.** Tofighi-Niaki et al. [61] investigated the nonlinear responses related to a rub between a journal and its bearing, in mixed lubrication. The rubbing phenomenon was considered in the TPJB model by modeling the surface roughness of both journal and bearing pads. The contact force between two rough surfaces, which is caused by the rubbing, was calculated based on the Hertz contact theory. The rotor response is presented with phase plane orbits, Poincaré maps, waterfall plots, and bifurcation diagrams and shows subharmonic, quasiperiodic, and chaotic motions. The authors state that abrupt increases and decreases in the impact force lead to qualitative changes in the rotor response. This implies that bifurcations may occur between two coexisting solutions, following an impact.

**1.7 Herringbone Groove Bearing.** The herringbone groove bearing has advantages over a plain journal bearing, namely in reducing side leakage and being free from whirl instability. Jang and Yoon [62] examined the dynamic characteristics of the herringbone groove bearing, solving Reynolds equation with finite element method (FEM). They verified that for the grooved journal case there exists excitation frequencies which corresponds to the operating speed multiplied by the number of grooves. Wang et al. [63] performed a numerical study of the nonlinear response attributed to a herringbone groove gas bearing and confirmed the existence of the periodic and quasiperiodic motions. Wang et al. [64] used computational fluid dynamics (CFD) and FEM techniques to consider

the fluid-structure interactions of the bearing. They demonstrated the improved dynamic stability of the herringbone groove gas bearing over the plain gas bearing.

**1.8 Non-Newtonian Fluid.** Newtonian lubricant is often mixed with an additive to adjust the bearing performance, producing a nonlinear relationship between the shear strain rate and shear stress. Sinhasan and Goyal [65] compared linear and nonlinear approaches to investigate the dynamic stability characteristics of a plain journal bearing with non-Newtonian fluid. They demonstrated how a linear lubricant bearing model yielded stable response, whereas the full nonlinear bearing model resulted in an instability (limit cycle). Jagadeesha et al. [66] analyzed the combined impact of the three-dimensional (3D) surface roughness and the non-Newtonian lubricant and showed that the non-Newtonian fluid reduces the minimum film thickness ratio compared with the Newtonian fluid. Kushare and Sharma [67] examined the effect of the non-Newtonian fluid on the dynamic stability of the worn hybrid journal bearing. They proved that the nonlinear non-Newtonian fluid has a very significant effect on the vibration orbits and system stability, especially under low load conditions.

**1.9 Turbulence in the Bearing Fluid Film.** Increasing needs for high rpm and usage of low viscosity lubricants has resulted in operating machinery with considerable turbulence in their hydrodynamic bearings. Hashimoto et al. [68] verified that turbulence in a fluid film bearing had a considerable effect on rotordynamic stability, utilizing short bearing theory and a turbulence coefficient for the bearing modeling.

Wang and Khonsari [29] applied HBT to obtain analytical expressions for the dynamic coefficients considering turbulence and showed that turbulence has a significant impact on the threshold speed of stability when the Sommerfeld number is lower than 0.3. Okabe and Cavalca [69] used short bearing theory to investigate the effect of turbulence on the dynamic behavior of a rigid rotor supported on tilting pad journal bearings. They demonstrated that turbulence effects modify the journal locus compared with the laminar condition model, and this trend was most evident at higher operating speeds. In addition, they showed that increasing the number of pads to 10 or 12 yielded a Hopf bifurcation into a limit cycle.

The remainder of this paper is arranged into the following sections: Sec. 2 provides sources and modeling methods for nonlinearity in bearings, Sec. 3 introduces solution methods and programming techniques for NL rotordynamics, Sec. 4 provides a summary of some presentation tools for NL phenomena in rotor-bearings, Sec. 5 provides examples that illustrate concepts introduced in the review paper and Sec. 6 summarizes and discusses future work.

## 2 Nonlinear Modeling of Thermo-Elasto-Hydro-Dynamic Bearing

Thermal and elastic effects in a journal bearing may have a significant influence on the overall rotordynamic response of a machine by modifying the thin fluid film thickness, lubricant viscosity, etc. In addition, time-varying aspects of the coupled thermal state of the fluid film, shaft and bearing structures can also cause thermally induced, synchronous instability (Morton effect). Due to its potentially high impact on rotor-bearing system response, TEHD aspects of the nonlinear journal bearing have been extensively researched for various applications, i.e., engine bearing, Morton effect, bearing seizure, etc.

**2.1 Engine Bearing.** Transient TEHD simulation approaches were widely developed in engine bearing applications [70–74], which involves a deformable connecting rod structure and is typically subject to high dynamic loading. Piffeteau et al. [74] researched the thermoelastic deformation effect on a connecting rod bearing using a two-dimensional (2D) finite element model of the rod. Two different thermal boundary conditions (adiabatic and isothermal conditions) were imposed on the outer surface of the connecting rod, and large differences between two cases in bearing performances resulted. This confirmed a necessity for TEHD modeling for engine bearing simulations. Kim and Kim [73] investigated transient TEHD responses of the connecting rod bearing model using a 3D finite element model. They found that thermal deformation is as important as elastic deformation in bearing performance prediction including minimum film thickness and oil flowrate. Fatu et al. [72] conducted transient TEHD engine bearing simulations and applied a new modeling approach for the temperature prediction of a fluid film using a second-order polynomial approximation for film temperatures. The predicted temperature using the method was validated with experimental results.

**2.2 Morton Effect.** The ME is a thermally induced instability problem which is caused by thermal bow of a shaft, resulting from viscous heating of the journal by the lubricant. A TEHD model is essential for simulating the Morton effect. Childs and Saha [75] and Lee and Palazzolo [76] used a 2D energy equation to develop a numerical model to predict the ME instability. Later, Suh and Palazzolo [7,8] demonstrated that using the 2D energy equation for film temperature prediction overpredicts the peak journal temperature differential when as compared with a 3D energy equation model. They further advanced their nonlinear transient ME prediction approach for a single overhung-shaped rotor, with the inclusion of the 3D energy equation, an asymmetric thermal expansion of the shaft, and thermal expansion of the TPJB pads. The numerical model was validated by comparison with available ME case histories, and demonstrated that thermal expansion effects significantly influence the ME. Tong and Palazzolo [77] used a hybrid beam-solid element method of the journal area as illustrated in Fig. 1, for thermal bow prediction resulting from asymmetric journal heating. They expanded their prediction model to cover ME problems arising in double overhung rotors and gas bearing applications [55,56,78]. Numerous parametric studies including bearing radial clearance, overhung mass, supply oil temperature, etc. were conducted to show their effects on the ME.

**2.3 Bearing Seizure.** Another thermally induced problem for rotors supported by hydrodynamic bearings is bearing seizure caused by an excessive reduction of bearing clearance due to the thermal expansion. Transient TEHD simulation is required for seizure prediction since the problem is typically observed during a rotor start-up condition. Monmousseau et al. [38] conducted a transient TEHD simulation of a TPJB under a rapid acceleration condition. They verified the accuracy of their model with experimental results and found that thermal expansion of the shaft is the main cause for bearing-journal seizure. The locations of minimum film thickness were found to be near the pivot positions due to the thermal expansion of the shaft. Monmousseau and Fillon [79] used simulation models to show that rotor acceleration rate is the critical factor for safe operation, free from seizure. Their results exhibited stable dynamic response of the rotor with slow acceleration, while a rapid decrease of bearing clearance was observed with higher rotor acceleration.

**2.4 Governing Fluid, Thermal and Elastic Bearing Equations With Nonlinear Terms.** Numerous modeling approaches have been used to obtain the hydrodynamic force of a fluid film bearing. A generalized Reynolds equation coupled with an energy equation is typically used to consider the thermal effect. The Reynolds equation is formed from the fluid momentum and continuity laws, and is used to predict pressure and velocity distributions in the fluid film. Equations (1) and (2) provide a common form of the Reynold's equation. This form neglects fluid inertia/shaft curvature, and considers an incompressible Newtonian fluid

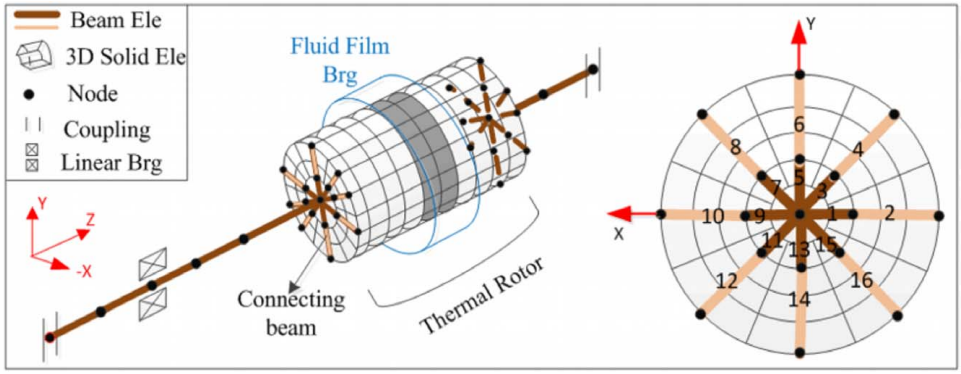


**Fig. 1 Diagram of hybrid beam-solid element method for thermal bow prediction [77]**

with variable fluid viscosity. The derivation assumes a laminar flow, uniform pressure distribution in the direction of film thickness, constant fluid density, and temperature-governed variable viscosity. Note that the bearing is assumed stationary, while the shaft surface velocity has the tangential and axial components [$\omega R$, 0], respectively

$$\nabla \cdot (C_1 \nabla P) + \nabla D_2 \cdot U + \partial h/\partial t = 0 \tag{1}$$

where $R$ is the journal radius, and $C_1$ and $C_2$ are constants related with the variable viscosity $\mu$

$$\begin{aligned} C_1 &= \int_0^h \int_0^z (\xi/\mu) d\xi dz - C_2 \int_0^h (\xi/\mu) d\xi, \\ C_2 &= \int_0^h \int_0^z (1/\mu) d\xi dz / \int_0^h (1/\mu) d\xi \end{aligned} \tag{2}$$

where $z$ is the axial coordinate of the fluid film bearing.

**2.5 Thermal Effect and Modeling.** The temperature distribution of a fluid film bearing plays a crucial role in accurately predicting the nonlinear dynamics of a rotor-bearing system since the variable lubricant viscosity coupled with the fluid film temperature affects the hydrodynamic force and the performances of the fluid film bearing. In addition, for Morton effect analysis, the fluid film temperature variation affects the thermal bow amplitude of the rotor, which may cause thermally induced vibration in the system. Great efforts have been devoted to investigating the thermal effect on the nonlinear behavior of rotor-bearing systems. Paranjpe and Han [70] conducted a transient THD simulation of a PJB subjected to dynamic loads, and using a full 3D energy equation and an Elrod cavitation algorithm. They analyzed the thermal time scales of a fluid film, a journal, and a bearing bushing and found that the time scales of the journal and the bushing are much greater than that of the fluid film. Paranjpe [71] compared two computationally efficient transient THD approaches: an adiabatic and a simplified thermal. The effective oil temperature was estimated considering power loss, oil mass flowrate, and temperatures at the inlet and outlet. It was shown that both the adiabatic and simplified models yield quite accurate predictions, with low computational costs. Gadangi and Palazzolo [80] and Gadangi et al. [81] performed a transient THD analysis of a tilting pad journal bearing (TPJB) using a 2D energy equation by calculating steady-state solutions for fluid temperature at each time-step. They verified that an isothermal fluid film model may produce significant errors in rotor-bearing response predictions, in particular for orbit size and minimum film thickness, by comparison with their THD model results. Monmousseau et al. [82] investigated transient thermal effect for a TPJB under dynamic loading conditions. They showed that the period of thermal transient process is much greater than that of mechanical transient, and it depends on the amplitude of the applied dynamic load. The difference between the periods is more significant when the amplitude of a dynamic load exceeds that of a static load. Monmousseau and Fillon [83] evaluated the frequency effect of a dynamic load and verified the existence of the thermal transient regime based on theoretical works. Simulated bearing temperature and dynamic response fluctuations became more evident with higher dynamic force frequencies.

Accurate prediction models of the thermal effect are highly desired for transient rotordynamic simulations, considering the high impact of fluid film temperature on bearing force predictions. A form of the energy equation is used in TEHD models to obtain the fluid film temperature distribution. Fluid film velocities are required to solve the energy equation, and are obtained from the Reynolds equation solution for pressures. The energy equation and Reynolds equation are coupled by the fluid velocities and by the variable viscosity term which is a function of fluid film temperatures. Various simplified forms of the energy equation have been proposed to calculate fluid film temperatures, due to the high computational costs of solving the energy equation in a transient simulation.

Fatu et al. [72] utilized a simplified energy equation for engine bearing modeling, by assuming a parabolic film temperature distribution along the film thickness direction. The second-order polynomial form of temperature approximation was used and compared well with experimental measurements. Paranjpe [71] presented a single effective viscosity method to simplify the THD analysis of an engine bearing model. The effective viscosity was obtained from the power loss, the mass flowrate of the oil and the pad's inlet and outlet temperatures. The viscosity value was obtained via an iterative method, and comparison between the simplified model and the 3D energy equation revealed that the suggested method can predict the film temperature reasonably well for the main bearing compared with the connecting rod, which has a very low oil supply through the oil feed hole in the journal. Fillon et al. [84] developed another single effective viscosity method which defines the effective temperature of a fluid film as a function of the oil temperature increase, and the film temperature at the leading edge. The effective viscosity model tended to overpredict the journal orbit size and maximum pressure. A simplified 1D energy equation was used in the nonlinear bifurcation analysis of a floating ring bearing by Kim and Palazzolo [85], in order to improve computational efficiency. The simplified energy equation was used to conduct a time-consuming nonlinear bifurcation analysis, by neglecting the temperature gradients in the axial and film thickness directions in order to reduce computation time. The Trigonometric Collocation Method was also implemented to obtain the lubricant temperatures.

The full 3D energy equation including temperature gradients in all of the journal's circumferential, axial, and radial directions ensures the most accurate prediction results in transient THD simulations. The energy equation in Eq. (3) is solved using the finite

element or other computational method, to obtain the 3D temperature distribution $T$ in the fluid film

$$\rho c\left(u\frac{\partial T}{\partial x}+w\frac{\partial T}{\partial z}\right)=k\left(\frac{\partial^2 T}{\partial x^2}+\frac{\partial^2 T}{\partial y^2}+\frac{\partial^2 T}{\partial z^2}\right)+\mu\left[\left(\frac{\partial \mu}{\partial y}\right)^2+\left(\frac{\partial w}{\partial y}\right)^2\right] \tag{3}$$

where $\rho$, $c$, and $k$ represent density, heat capacity, and heat conductivity, respectively, and $u$, $v$, and $w$ represent the fluid velocities in the circumferential, film thickness, and bearing axial directions, respectively. Mixing theory is typically utilized to obtain approximate pad inlet temperatures for boundary conditions on the energy equation. Paranjpe and Han [70] utilized the 3D energy equation for engine bearing research, and emphasized the necessity of including the time-dependent film thickness. Suh and Palazzolo [7,8] further improved the accuracy of the thermal effect model by using the 3D energy equation and incorporating the time-dependent thermal expansion of pads and shaft in the film thickness calculation. A quadratic up-winding scheme was used to avoid spatial temperature oscillations due to the convection term.

The use of the 3D energy equation was expanded to transient ME simulation of a gas bearing-supported rotor in Tong and Palazzolo [78]. This required a different variable viscosity form in the energy equation. The 2D Energy equation [38,58–60,73,75,76,80–84,86,87] presents a good alternative for the 3D Energy equation to reduce the complexity of model and the computation time. In the 2D version, the temperature gradient in the bearing's axial direction is neglected, and the film temperature is predicted at the bearing mid-plane. However, as demonstrated by Suh and Palazzolo [7,8], when it is used for the ME prediction, the 2D version overpredicts the journal temperature differential in the circumferential direction significantly compared with the 3D version.

**2.6 Bearing's Elastic and Thermal Deformation Effect and Modeling.** The deformation of bearing pads induced by elastic and thermal effects also has a direct impact on the nonlinear responses of a rotor system. Suh and Palazzolo [7,8] incorporated a flexible pad effect into the TPJB model and showed that the elastic pad effect induces a relatively larger orbit size and increased maximum fluidic pressure. Fillon et al. [84] compared both the transient THD and TEHD simulation models and verified that considering only thermal effect may overpredict the journal orbit size and the maximum pressure of the TPJB. In their research, the thermal expansion effect was also considered, and the effect was found to be more dominant in the bearing performance compared with the elastic deformation effect in the low dynamic load case. Monmousseau et al. [26] showed good agreement between experimental results and a TEHD TPJB model, including fluid film thermal effect, thermal and elastic deformations of pads, and pivot deflection. It was confirmed that more accurate predictions can be achieved when both the thermal and elastic deformations are considered compared with the thermal effect only case. Kucinschi et al. [86] analyzed the thermal transient of a steadily loaded plain journal bearing using the thermoelastic deformation model. The prediction model was compared with the experimental results, and reasonable agreement between two were observed.

One-dimensional (1D) analytic, 2D, and 3D FEM methods have been used for including the pad's elastic deformation effect in the transient EHD analysis. Monmousseau et al. [26] adopted the analytic method for calculating the pad deformation based on the plane strain hypothesis by Nilsson [88]. In the method, the pad deformation in pad's radial direction is calculated based on the hydrodynamic pressure imposed on the pad's inner surface. To incorporate more detailed pad deformation model into the bearing model, Desbordes et al. [89] suggested a 2D plane strain finite element (FE) model. For this approach, the fluid's pressure force was obtained by solving Reynolds equation, and averaged along the bearing axial direction. The force was then applied on the pad inner surface as a boundary condition. A 3D elastic pad model was utilized in the actively operated TPJB model of Haugaard and Santos [57] and the ME—TPJB model of Suh and Palazzolo [8]. The latter incorporated the stiffness and damping matrix of the pad into the bearing dynamics model, and numerically integrated the coupled equations for the pads and rotor in the time-domain, using the Runge–Kutta method. This approach removes the Newton–Raphson (NR) iteration process for determining the static equilibrium positions of the journal and pads but requires more computation time for the numerical integration. They adopted a modal reduction technique to reduce the computational costs.

Another important aspect that has a significant, but indirect, effect on the nonlinear behavior of the rotor system is the thermal expansions of the shaft and bearing pads. Monmousseau et al. [38] verified that thermal expansion has a more dominant effect than elastic deformation in bearing seizure prediction. Monmousseau et al. [26] included the thermal expansion effect of the shaft, the pads, and the housing in the radial direction. The radial expansion of the structures was obtained utilizing plane stress models and assuming that the pad freely expands. More rigorous thermal expansion models using 3D FE models of the pads and the shaft were developed by Suh and Palazzolo [7,8] for ME modeling as shown

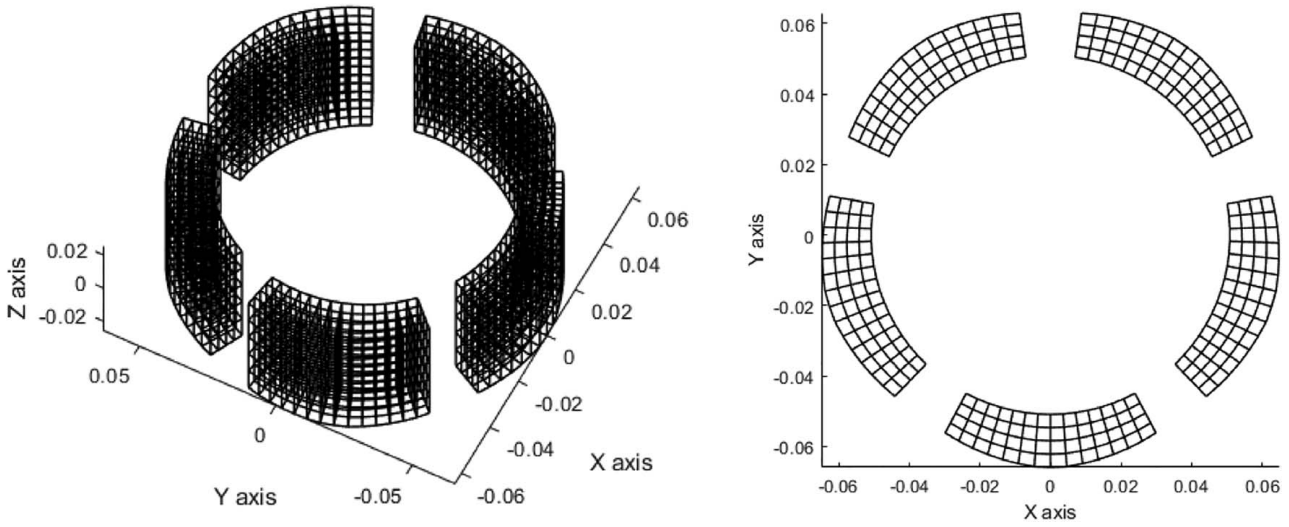


**Fig. 2 3D FE model of TPJB Pads**

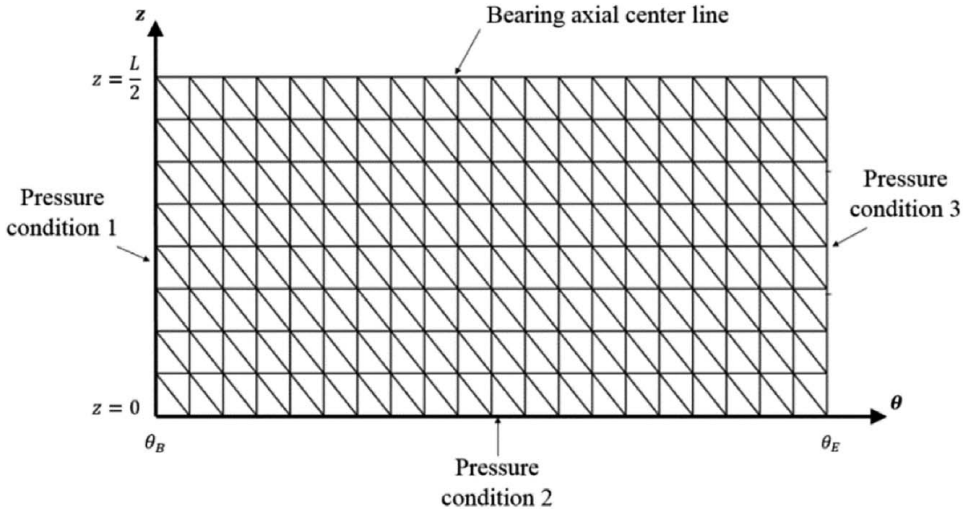


**Fig. 3 Pressure and flow boundary conditions on a bearing pad model**

in Fig. 2. The thermal expansions of the shaft and bearing were determined by solving the 3D FE model stiffness equation as

$$[\boldsymbol{K}_{\Delta T}][\mathbf{D}_{\Delta T}] = [\mathbf{F}_{\Delta T}] \tag{4}$$

where $\mathbf{D}_{\Delta T}$ is the nodal displacement vector in the $x$, $y$, and $z$ directions resulting from the thermal load vector $\mathbf{F}_{\Delta T}$. The latter is generated from the shaft and bearing temperature distributions. In the method, the nodes at the shaft ends were set to feely move in the axial direction. The displacements due to thermal expansion were obtained at each 3D node, and applied for updating the film thickness, to consider the asymmetric thermal expansion of the shaft in both the circumferential and axial directions.

**2.7 Bearing Boundary Conditions.** Pressure boundary conditions are imposed on the finite-length bearing model's FEM mesh according to the particular bearing configuration. An example for pressure boundary conditions is shown in Fig. 3. A half symmetry fluid film pressure distribution is typically assumed, when the thermal effect is excluded in the bearing model. Therefore, only one half of the bearing is meshed in the figure. The symbols $z$ and $\Theta$ represent the bearing axial and circumferential directions, respectively, and $L$, $\Theta_{\mathrm{B}}$, and $\Theta_{\mathrm{E}}$ are the bearing length, and the beginning and end angular positions of the bearing pad, respectively. Pressure boundary conditions are applied to the bearing axial end ($z = 0$) and bearing side surfaces ($\Theta = \Theta_{\mathrm{B}}$, $\Theta = \Theta_{\mathrm{E}}$).

The pressure boundary conditions can apply ambient pressure, oil supply pressure, or pressure continuity in a plain journal bearing. Thermal boundary conditions are also required for THD and TEHD bearing models. The thermal boundary conditions used in the ME research [7,8] is presented in Fig. 4. Boundary conditions are imposed for the interfaces between the lubricant and bearing pad/journal surfaces.

The heat flux and temperature boundary conditions are applied between the lubricant and the bearing pad, and are shown in Eq. (5). For the lubricant/journal interfaces, the rotational motion of the shaft needs to be accounted for and the boundary conditions are shown in Eq. (6)

$$\left.k_L \frac{\partial T_L}{\partial r}\right|_{r=R+H} = \left.k_B \frac{\partial T_B}{\partial r}\right|_{r=R+H}$$
$$T_L|_{r=R+H} = T_B|_{r=R+H} \tag{5}$$

$$\left.k_L \frac{\partial T_L}{\partial r}\right|_{\theta=0,\, r=R} = \left.k_J \frac{\partial T_J}{\partial r}\right|_{\theta=-\omega t,\, r=R}$$
$$T_L|_{\theta=0,\, r=R} = T_J|_{\theta=-\omega t,\, r=R} \tag{6}$$

**2.8 Rotordynamic Modeling.** A Jeffcott rotor model is widely used for its ability to demonstrate important qualitative features of more complex rotordynamic shaft models, and its high computational efficiency. The equations for the Jeffcott rotor supported with tilting pad journal bearing are

$$\begin{aligned} M_{pad\_i}\ddot{y}_{pvt} &= -K_P y_{pvt} + F_{pad\_i} \\ I_{tilt\_i}\ddot{\delta}_{tilt} &= MO_{tilt\_i} \\ I_{roll\_i}\ddot{\alpha}_{roll} &= MO_{roll\_i} \\ I_{yaw\_i}\ddot{\beta}_{yaw} &= MO_{yaw\_i} \end{aligned} \tag{7}$$

where $i$ represents the pad number, $M_{pad\_i}$, $I_{tilt\_i}$, $I_{roll\_i}$, and $I_{yaw\_i}$ are the mass of pad and the tilting/rolling/yawing inertias of the pad, respectively. The terms $F_{pad\_i}$, $MO_{tilt\_i}$, $MO_{pitch\_i}$, and $MO_{yaw\_i}$ are the fluid film force and the tilting/rolling/yawing moments applied to a pad, respectively. These values are obtained from solving the Reynolds Eq. (1).

Euler or Timoshenko beam elements can be utilized in a finite element model of the shafting, for an improved lateral rotordynamics model relative to the Jeffcott rotor model. The dynamic equations of the rotor system then become

$$[\dot{\mathbf{U}}] = [\mathbf{D}][\mathbf{U}] + [\mathbf{F}] \tag{8}$$

where $[\mathbf{U}] = \begin{bmatrix} \dot{\mathbf{Z}} \\ \mathbf{Z} \end{bmatrix}$, $[\mathbf{D}] = \begin{bmatrix} -\mathbf{M}_{ro}^{-1}\mathbf{C}_{ro} & -\mathbf{M}_{ro}^{-1}\mathbf{K}_{ro} \\ \mathbf{I} & \mathbf{0} \end{bmatrix}$, $[\mathbf{F}] = \begin{bmatrix} \mathbf{M}_{ro}^{-1}\mathbf{F}_{ro} \\ \mathbf{0} \end{bmatrix}$

$\mathbf{U}$, $\mathbf{M}_{ro}$, $\mathbf{C}_{ro}$, and $\mathbf{K}_{ro}$ are the rotor's state vector, mass, damping, and stiffness matrices, respectively. The term $\mathbf{F}_{ro}$ is the force vector including the nonlinear hydrodynamic force from the fluid film bearings, the unbalance force, weight, etc. Using a beam FEM model for transient rotordynamic simulation requires high computational costs. Therefore, a modal reduction technique is adopted to reduce the system's degree of freedom. The biorthogonality of the right and left eigenvectors ($\psi_R$, $\psi_L$) with respect to the matrix [**D**], is used to diagonalize the governing equations yielding the "modal" coordinate equations

$$[\dot{\mathbf{Y}}] = [\mathbf{A}][\mathbf{Y}] + [\psi_L^T][\mathbf{F}] \tag{9}$$

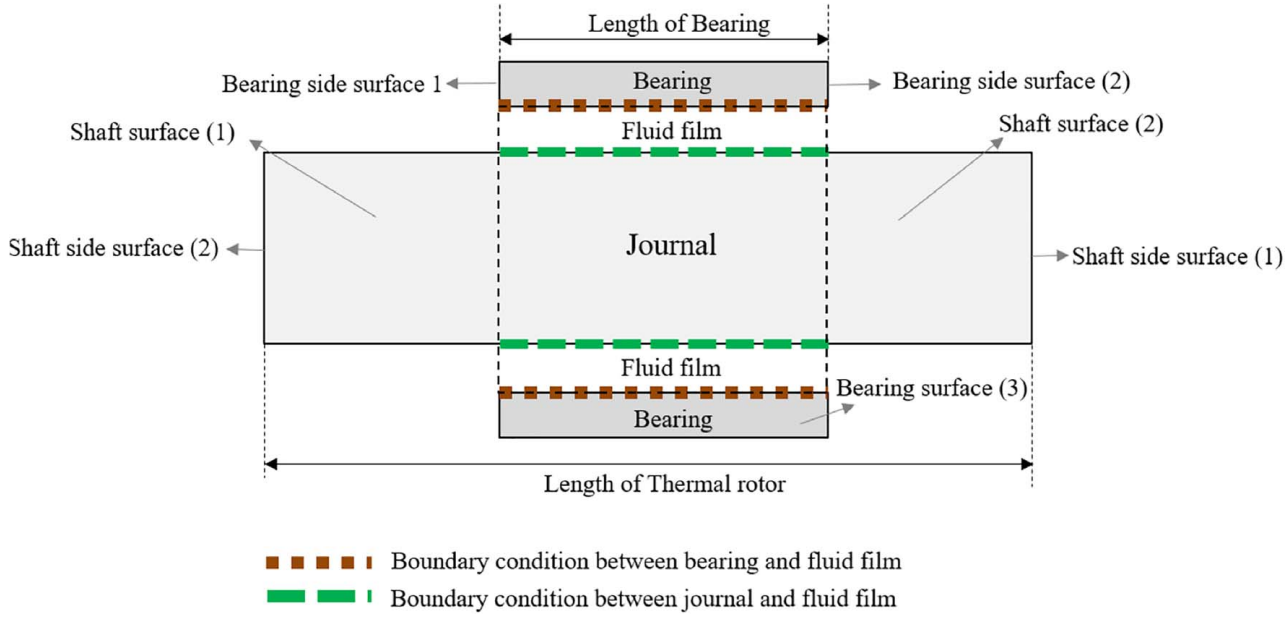


**Fig. 4 Thermal boundary conditions on rotor and bearing surfaces**

where $[\mathbf{Y}] = [\psi_R][\mathbf{U}]$, $[\mathbf{A}] = [\psi_{Lm}^T][\mathbf{D}][\psi_{Rm}] = \begin{cases} \lambda_i & \text{if } m = n \\ 0 & \text{if } m \neq n \end{cases}$

$\lambda_i$ is the $i$th eigenvalue of the system. Generally, only a small number of modal coordinates need be utilized to obtain converged results for the rotordynamic system's transient response.

## 3 Solution Methods

There exist very few closed form analytic solutions to nonlinear dynamics problems of practical interest. The alternatives are approximate solutions and numerically integrated solutions. The former usually involves representing the solution in terms of truncated trigonometric series which yields sets of nonlinear algebraic equations, utilizing recursive techniques such as multiple time scales, or posing the problem in terms of time averaged variables. The latter approach may involve numerically integrating to steady state with arbitrary initial conditions which is referred to as a TNI or incorporating an algorithm that provides initial conditions directed toward locating coexisting steady-state, periodic solutions, which is referred to as a direct search numerical integration.

**3.1 Transient Numerical Integrations.** Transient numerical integration provides a reliable means of obtaining the response of a nonlinear system to initial conditions and external forcing, given an effective NI approach and time-step selection. It remains the sole means for determining aperiodic and chaotic responses, and for determining Lyapunov exponents to identify chaos in continuous time systems. Its shortcoming is in selecting initial conditions that will yield multiple coexisting steady-state solutions.

Suppose that the governing equations for the dynamic system are posed in standard second-order form, and then transformed to first order form by using velocities as well as displacements as state variables. The result is

$$\begin{bmatrix} \mathbf{M} & \mathbf{0} \\ \mathbf{0} & -\mathbf{K} \end{bmatrix} \begin{Bmatrix} \ddot{\mathbf{x}} \\ \dot{\mathbf{x}} \end{Bmatrix} + \begin{bmatrix} \mathbf{C} & \mathbf{K} \\ \mathbf{K} & \mathbf{0} \end{bmatrix} \begin{Bmatrix} \dot{\mathbf{x}} \\ \mathbf{x} \end{Bmatrix} = \begin{Bmatrix} \mathbf{F} \\ \mathbf{0} \end{Bmatrix} \tag{10}$$

or

$$\mathbf{A}\dot{z} + \mathbf{B}\mathbf{z} = \hat{\mathbf{F}} \tag{11}$$

where $\mathbf{F}$ contains the nonlinear bearing forces. Premultiplication of Eq. (11) by the inverse of $\mathbf{A}$ yields

$$\begin{Bmatrix} \ddot{\mathbf{x}} \\ \dot{\mathbf{x}} \end{Bmatrix} = \begin{bmatrix} -\mathbf{M}^{-1}\mathbf{C} & -\mathbf{M}^{-1}\mathbf{K} \\ \mathbf{I}_N & \mathbf{0} \end{bmatrix} \begin{Bmatrix} \dot{\mathbf{x}} \\ \mathbf{x} \end{Bmatrix} + \begin{Bmatrix} \mathbf{M}^{-1}\mathbf{F} \\ \mathbf{0} \end{Bmatrix} \tag{12}$$

or

$$\dot{\mathbf{z}} = \mathbf{D}\mathbf{z} + \tilde{\mathbf{F}}, \quad \mathbf{z}(0) = \mathbf{z}_0 \tag{13}$$

The first-order differential equation form of Eq. (13), including initial conditions, is amenable to numerical integration with Euler's method, Runge-Kutta, etc. The form in (13) may include time-varying coefficients (parametric excitation) or nonlinear bearing forces, whether explicit such as obtained from short bearing theory, or implicit as obtained from finite bearing theory using for example the FEM to solve Reynold's equation. The form in (13) may also contain a parameter which when varied can cause a response bifurcation, the most common being the vibration jump phenomena which occurs in response to varying the speed of an unbalanced rotor.

The TNI approach extends to a pre-assigned final time at which point the response may become periodic, aperiodic or chaotic. TNI is generally the most common approach for solving nonlinear rotordynamic equations of motion. This is more the case for very large order systems which may include TEHD effects. Gadangi and Palazzolo [80] and Gadangi et al. [81] utilized TNI to predict the time transient response for a shaft supported on TEHD modeled, nonlinear, tilting pad journal bearings and subjected to a sudden imbalance due to blade or deposit loss. Suh and Palazzolo [7,8] utilized TNI to predict the time transient response of a high fidelity, NL, Morton effect (i.e., thermal induced synchronous instability) model, including 3D structural finite elements for the shaft and pads, and variable viscosity Reynolds fluid film model with a transient energy equation. Clarke et al. [6] utilized TNI for rotordynamic simulation with FRB modeled with a steady-state thermal model with π oil films. They considered heavily loaded power generating systems and compared results with isothermal models. Holt et al. [13] utilized TNI for simulating a lightly loaded turbocharger utilizing an advanced lumped parameter thermal model, and compared results with experimentally measured results.

**3.2 Direct Search Algorithms: Assumed Periodic Approximate Form Approach.** Unlike the TNI, DSA methodically search for multiple coexisting solutions of the NL dynamical system. DSA can be roughly categorized into two general approaches: the APAF approach and the APNIF approach.

*3.2.1 Assumed Periodic Approximate Form: Harmonic Balance Approach.* The HBM is a commonly used APAF approach. It is usually utilized for obtaining the natural frequency and multiple, coexisting forced harmonic responses of NL systems. The general form for the NL system governing equation may be expressed as

$$\frac{d^2\mathbf{x}}{dt^2} + \mathbf{Q}\left(\mathbf{x}, \frac{d\mathbf{x}}{dt}\right) = 0 \tag{14}$$

Harmonic balance method assumes the response of the NL system may be represented by the truncated Fourier series:

$$\mathbf{x} = \mathbf{a}_0 + \sum_{j=1}^{m} [\mathbf{a}_j \cos(j\omega t) + \mathbf{b}_j \sin(j\omega t)] \tag{15}$$

where $\omega$ is the fundamental frequency is defined as

$$\omega = 2\pi/T \tag{16}$$

where $T$ is the fundamental oscillation period. The approximation for $x(t)$ in Eq. (15) is substituted into Eq. (14), and the resulting powers of sin and cos are converted into linear sin and cos terms involving higher harmonics. Grouping like harmonics and invoking the linear independence of sin and cos terms yields a set of nonlinear algebraic equations for the unknowns $\mathbf{a}_0$, $\mathbf{a}_j$, and $\mathbf{b}_j$ constants in (15). These equations may be solved iteratively with MAPLE, MATLAB, etc. to obtain coexisting, approximate steady-state solutions. The stability of the coexisting solutions may be ascertained by linearizing the system, substituting the approximate solution, and then applying Floquet theory to the resulting linear differential equations with time harmonic coefficients.

Harmonic balance method is widely used for NL rotordynamic problems including bearing clearance [16], squeeze film damper [27,90], rub/contact [20], and dead-band clearance in ball bearing [19]. As a result, harmonic and sub-/super-harmonic solutions were predicted and plotted versus system parameters. HBM was used in conjunction with discrete Fourier transform (DFT) and inverse DFT procedures to model complicated NL force functions [17–19,91,92].

*3.2.2 Assumed Periodic Approximate Form: Trigonometric Collocation Method.* The TCM was developed and formalized by Samoilenko and Ronto in 1979 as the method of periodic successive approximations [93]. Nataraj and Nelson [21] applied the TCM for NL rotordynamic problems, including a flexible rotor supported with squeeze film dampers. Similar to the HBM, the solution is approximated by a finite trigonometric series with $\omega$ as the fundamental frequency, as in Eqs. (15) and (16). The unknown coefficients of the above series are ordered into a vector

$$c_i = (a_{0i}, a_{1i}, b_{1i}, a_{2i}, b_{2i}, \cdots, a_{mi}, b_{mi}) \tag{17}$$

corresponding to the state variable $\mathbf{x}_i$. The TCM consists of substituting the assumed form of the solution (15) into the governing Eqs. (14), and requiring that the equations be identically satisfied at a specified number of times equally distributed in the period T. Jean and Nelson [22] introduced TCM that could be applied directly in physical coordinates for large order NL rotordynamic systems, with enhanced computational efficiency. Chinta and Palazzolo [28] also applied the TCM to a magnetic bearing system and successfully identified various periodic responses.

**3.3 Direct Search Algorithms: Assumed Periodic Numerically Integrated Form Approach**

*3.3.1 Hopf Bifurcation Theory.* The HBT approach yields conditions on a system parameter $\alpha$ which causes the system described by $\dot{\mathbf{x}} = \mathbf{f}(\mathbf{x},\alpha)$, to experience a bifurcation from a fixed equilibrium point to a limit cycle, as the parameter changes value. A complex conjugate pair of eigenvalues of the system, linearized at the fixed equilibrium point, experiences a transition from purely imaginary values to positive real part eigenvalues at the bifurcation. Though it is limited to smaller order systems, HBT provides the proper information for the prediction of the occurrence, shape and period of the periodic solution. Wang and Khonsari utilized HBT in a series of papers [29–33] investigating journal bearing system stability with respect to rotor stiffness, oil flow and oil temperature. Boyaci et al. [34] investigated Hopf bifurcation in a simple rigid rotor supported by floating ring bearing using HBT. They determined the stability region with respect to the operation parameters and distinguished the types of occurrence such as sub- and supercritical Hopf bifurcation using the center manifold theorem.

*3.3.2 The Shooting Method.* The shooting method is a general, numerical algorithm to identify periodic solutions of two-point boundary value problems. Vibrating systems have periodic solutions for the following three cases: (a) periodically excited systems (nonautonomous case), (b) undamped free vibration systems (autonomous case), and (c) small motion unstable—large motion stable limit cycle systems (autonomous case). In nonautonomous systems, the period of the response is typically a rational multiple of the known excitation period. The most common form of periodic excitation in rotating machinery is mass imbalance, which occurs at the shaft spin frequency. In contrast, the response period of autonomous systems is unknown and depends on its mass, stiffness, and damping characteristics. Thus, an additional equation is needed to augment the periodicity conditions [94] in seeking periodic responses. Numerical algorithms are presented for both autonomous and nonautonomous cases. Equation (18) expresses the fundamental condition of periodic response, where $\mathbf{x}_0$ represents an initial state vector and $\mathbf{x}_{TR}(\mathbf{x}_0, \tau)$ the same state vector at a later time $\tau$.

The response period is a typically a rational multiple of an excitation period $\tau_e$ in a nonautonomous system

$$f(\mathbf{x}_0, \tau) = \mathbf{x}_{TR}(\mathbf{x}_0, \tau) - \mathbf{x}_0 = 0 \tag{18}$$

The shooting algorithm utilizes NR to iteratively locate periodic states that satisfy Eq. (18) and is typically represented by

$$non-autonomous: \quad \mathbf{x}_0^{i+1} = \mathbf{x}_0^i + (\mathbf{J}_x^i - \mathbf{I})^{-1}(\mathbf{x}_o^i - \mathbf{x}_{TR}(\mathbf{x}_0^i)) \tag{19}$$

$$autonomous: \quad \begin{Bmatrix} \mathbf{x}_0^{i+1} \\ \tau^{i+1} \end{Bmatrix} = \begin{Bmatrix} \mathbf{x}_0^i \\ \tau^i \end{Bmatrix} + \begin{bmatrix} \mathbf{J}_x^i - \mathbf{I} & \mathbf{J}_\tau^i \\ \dot{\mathbf{x}}_0^{i^T} & \mathbf{0} \end{bmatrix}^{-1} \begin{Bmatrix} \mathbf{x}_0^i - \mathbf{x}_{TR}(x_0^i, \tau^i) \\ \mathbf{0} \end{Bmatrix} \tag{20}$$

where $\mathbf{J}_x = \dfrac{d\mathbf{f}}{d\mathbf{x}} = \left[\dfrac{\partial \mathbf{f}}{\partial x_1} \quad \cdots \quad \dfrac{\partial \mathbf{f}}{\partial x_n}\right], \quad \mathbf{J}_\tau = \dfrac{d\mathbf{f}}{d\tau}$

$\mathbf{J}_x$ and $\mathbf{J}_\tau$ represent Jacobian matrices with respect to phase states and period state, respectively. More detailed descriptions are available in Ref. [95]. In 1997, Sundararajan and Noah applied the shooting method to a rigid rotor supported on squeeze film damper (SFD) bearings [23], along with the CMS method [24] for a large order rotor-bearing system with local strong nonlinearity.

*3.3.3 Programming Techniques.* Increased demands for higher-fidelity rotordynamic system simulations have provided an impetus for the increased use of FEM/CFD in NL rotordynamic modeling. Much of the earlier work relied on simplified bearing models, such as infinitesimally short or infinitely long-bearing approximations, and rigid rotors, due to the computational burden of evaluating the Jacobian matrix each iteration. Thus, bearing

models were also limited to simpler geometries, such as plain journal or floating bushing bearings [23,24]. Kim and Palazzolo [35–37] developed computationally efficient means to implement the shooting method for complex bearing geometries and complex shafting, by utilizing a deflation algorithm and parallel computing strategy. As results, they were able to apply the shooting method to model rotordymanic systems including finite-length FRB and TPJB, with variable viscosity effects.

Deflation algorithms successively modify the mathematical model in the iterative search for coexisting solutions to avoid re-convergence to already located solutions of the NL system [96–98]. With the convergence to a new solution, the original system is modified to remove all previously found solutions, and avoid re-convergence to any already found solution. The deflated function $\mathbf{f}(\mathbf{x},\tau_0)$ includes a denominator term $h$, which is a series product of relative Euclidean norms of the previously found solution vector as

$$\begin{Bmatrix} \mathbf{x}_0^{i+1} \\ \tau^{i+1} \end{Bmatrix} = \begin{Bmatrix} \mathbf{x}_0^{i} \\ \tau^{i} \end{Bmatrix} + \begin{bmatrix} \mathbf{J}_x^i - \mathbf{I} & \mathbf{J}_\tau^i \\ \dot{\mathbf{x}}_0^{iT} & \mathbf{0} \end{bmatrix}^{-1} \begin{Bmatrix} \mathbf{x}_0^i - \mathbf{x}_{TR}(x_0^i,\ \tau^i) \\ \mathbf{0} \end{Bmatrix} \tag{21}$$

A second strategy for faster execution is the adoption of parallel computing methods [99,100]. Parallelized numerical routines for obtaining Jacobian matrices in the shooting algorithm can significantly reduce computation time, since the boundary value problems with perturbed initial conditions are decoupled from each other, and solved simultaneously. The multiple numerical time integrations required to form the Jacobian matrix are executed in parallel. The desired number of carriers, i.e., multi-processors, depends on the system states dimension and the shooting parameters. The parallel computing approach can also be used for any other perturbation-based search methods.

Figure 5 [36] depicts the flowchart of the improved shooting algorithm for rotordynamic systems. The highlighted sections of the chart designate the deflation and parallel computing techniques.

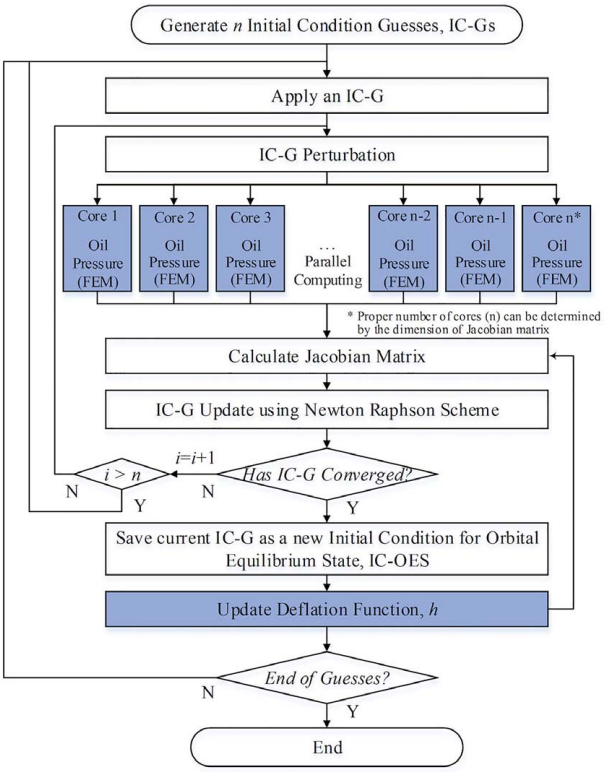


**Fig. 5 Flow diagram for parallel computing and deflation aided shooting [36]**

The efficiency of deflation and parallel computing is discussed in detail in Ref. [37].

*3.3.4 Numerical Continuation.* A numerical continuation is an algorithm which utilizes a system of parametrized nonlinear equations and an initial solution $(u_0,\ \lambda_0)$, such that $F(u_0,\ \lambda_0) = 0$, to produce a set of points on the solution curves. The parameter continuation approach can provide improved insights into the circumstances and occurrences of stable/critical point bifurcations, such as saddle-node, transcritical, pitch-fork, period doubling, Hopf, and secondary Hopf (Neimark) bifurcations. Parameter continuation also provides a more dependable system to analyze a dynamical system, as it is more stable than more interactive, time-stepped numerical solutions. Detailed mathematical descriptions of numerical continuation methods are provided in Ref. [95]. Numerical continuations were often applied to rotordynamic systems to plot solution states for varying parameter conditions such as operation speed, imbalance eccentricity, etc. Chouchane and Amamou [101,102] used MATCONT, an open access MATLAB numerical continuation package developed by Dhooge et al. [103,104]. They detected the Hopf bifurcation point along the bearing parameter of plain journal bearings, and TNI was used to support the results obtained by the continuation method. Boyaci et al. [105] presented entire solution branches including coexistent solution regions for a turbocharger rotor supported on FRBs, with respect to rotating speed. Kim and Palazzolo [35–37] accelerated the Jacobian calculation routine in arc-length continuation, by using parallel computing. This provided a practical means to utilize higher-fidelity finite-length models of FRB and TPJB in the bifurcation study. Groll and Ewins [20] combined numerical continuation with an HBM frequency domain solution search method, for rotor/stator contact problems, and demonstrated improved efficiency.

## 4 Nonlinear Response Presentations

**4.1 Nonchaotic Oscillations.** Various types of presentation formats have been developed to facilitate qualitative and quantitative insights and understanding of the underlying characteristics of nonlinear dynamical system response. These are discussed in the following text.

*4.1.1 Orbital Status and Frequency Components.* The lateral motion of the shaft and its frequency components provide a general means to examine stability, response severity, and causality associated with NL rotordynamic system dynamical response. The emergence of the limit cycle, single or multiple harmonics, quasiperiodic, and aperiodic motions can be intuitively distinguished with these two representative methods.

*4.1.2 Phase Portrait.* A phase portrait plots the trajectory of a state versus other states in a dynamical system. Typically, these trajectories are plotted for various initial states to show attractors, repellors, domains of attraction, limit cycles, and fixed equilibrium points. An attractor is a stable point which is also called a "sink." The repellor is considered as an unstable point, which is also known as a "source."

*4.1.3 Poincaré Section.* Plotting the response point (Poincaré dot) at consecutive periods, versus a system parameter provides a visual tool to identify bifurcations, subharmonic responses, etc. These dots are typically obtained from a direct NI solution of the governing equations of motion. Typically, the NI is performed for 100's or 1000's of periods prior to initiating the Poincaré section in order to present only steady-state solution results. The Poincaré section plots are typically provided for both increasing and decreasing changes of the system parameter. This reveals hysteresis and different bifurcations depending on the direction of the parameter change. Further insights may be gained by plotting "waterfall" frequency spectra with the third axis being the varying system

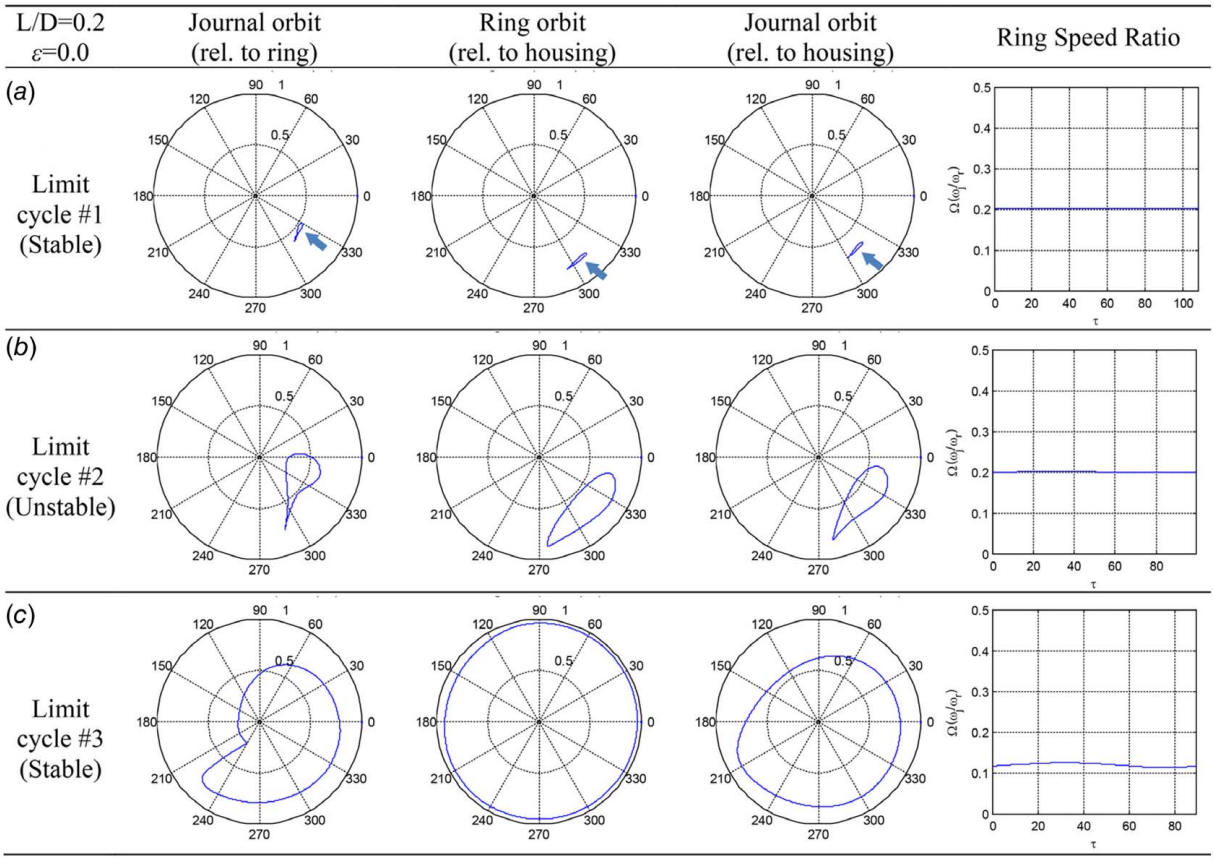


**Fig. 6 Identified coexisting responses using the shooting method at 80,000 rpm ($L/D = 0.2$): (*a*) limit cycle #1 (stable), (*b*) limit cycle #2 (unstable), and (c) limit cycle #3 (stable)**

parameter. This provides a greater understanding of the dot structure and trends in the Poincaré section.

*4.1.4 Solution Branches.* The solution branch diagram (SBD) provides an alternative presentation method for bifurcations, and is especially useful for presenting multiple coexistent solution cases. The maximum and minimum values of the nondimensional displacements, $y/C_b$, of the periodic solutions are plotted with respect to a control parameter in this diagram. The SBD is typically included with the numerical continuation method to illustrate (1) the emergence of periodic solutions and the growing/shrinking of orbital motions, (2) limit cycles or quasiperiodic or aperiodic

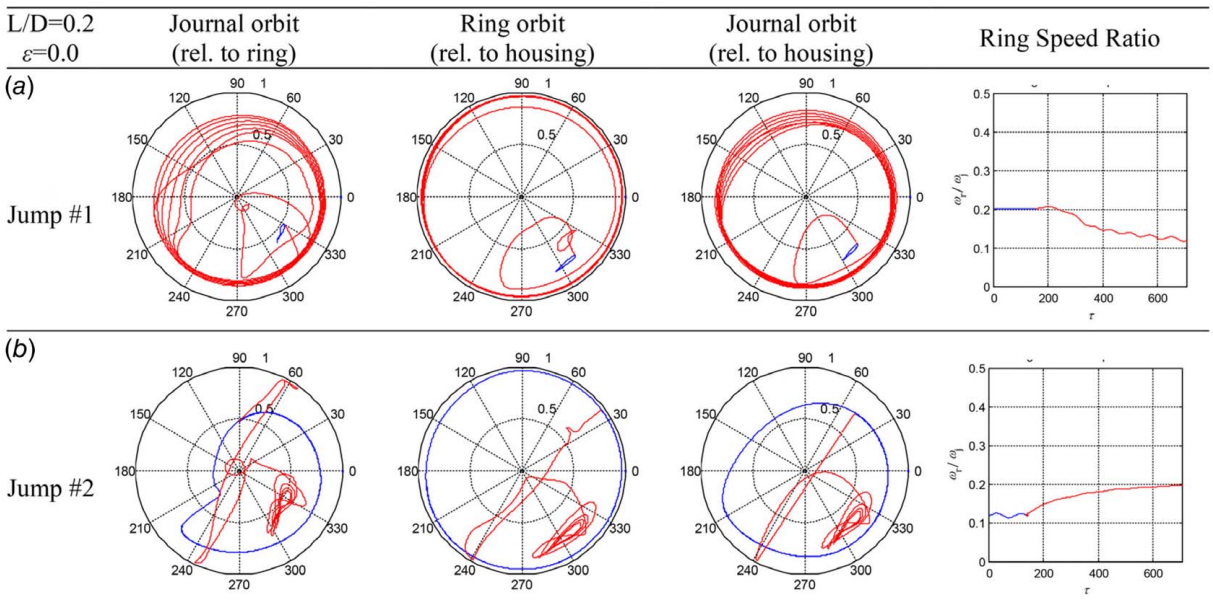


**Fig. 7 Jump phenomena between two limit cycles due to bump from FRB base at 80,000 rpm ($L/D = 0.2$, $\epsilon = 0.0$): (*a*) limit cycle #1 to limit cycle #3, (*b*) limit cycle #3 to limit cycle #1**

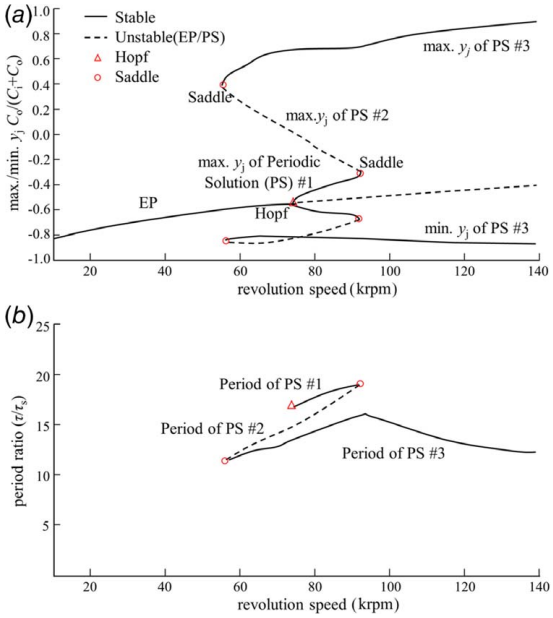


**Fig. 8 Bifurcation diagram ($L/D = 0.2$, $\epsilon = 0.0$) using numerical continuation: (*a*) revolution speed versus max/min $y_j$ and (*b*) revolution speed versus period ratio ($\tau/\tau_s$)**

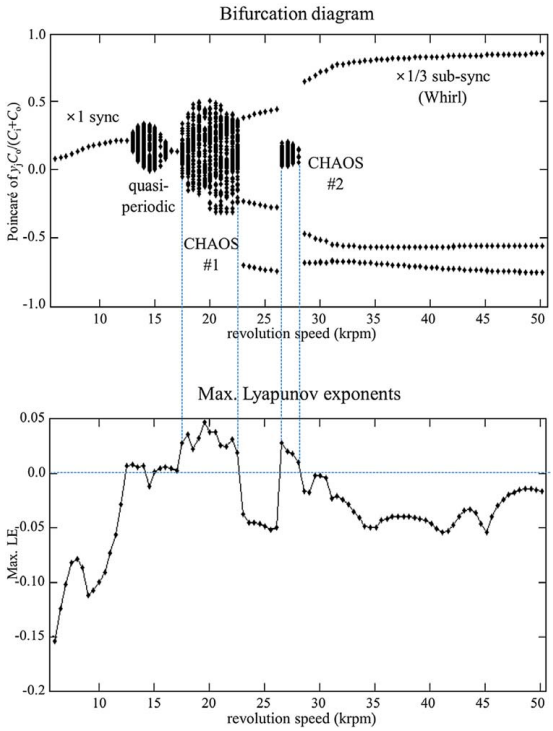


**Fig. 9 Bifurcation diagram (Poincaré section) and corresponding maximum LEs ($L/D = 0.2$, $\epsilon = 0.4$)**

motions without massive dots or lines, which may hide other coexisting solutions, and (3) sub-/supercritical types of Hopf bifurcation, Neimark-Sacker bifurcation and others.

**4.2 Chaotic Oscillations.** Nonlinear rotor-bearing systems may experience chaotic vibrations, especially when a bearing operates under heavy load and/or high speeds. Additional qualitative or quantitative presentation methods may be used in these cases.

*4.2.1 Strange Attractor.* The random nature of chaos requires presentation methods beyond those used for periodic or quasiperiodic motions. Poincaré maps of chaotic response typically reveals regularities in geometric shapes referred to as strange attractors. These typically include fractal or other complex patterns.

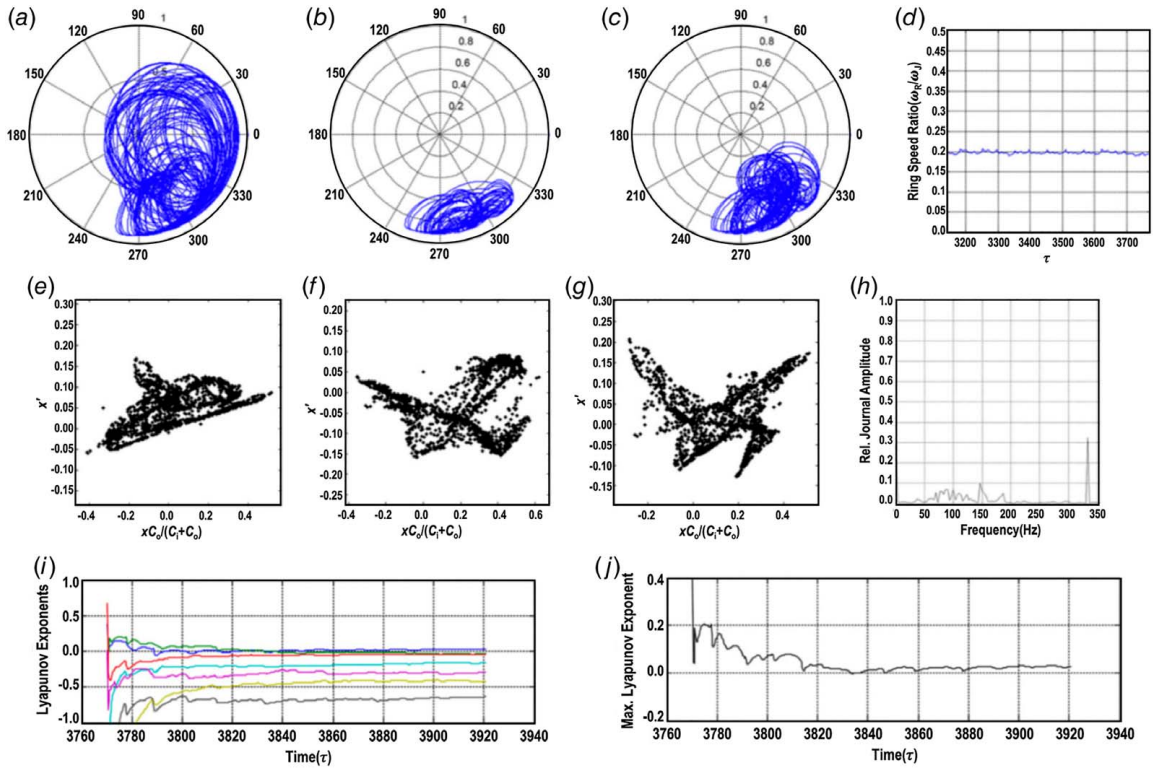


**Fig. 10 Nonlinear response evaluation at 20,000 rpm ($L/D = 0.2$, $\epsilon = 0.4$): (*a*)–(*d*) for orbits and ring speed, (*e*)–(*g*) for Poincaré maps, (*h*) for frequency spectrum, (*i*) for LEs, and (*j*) for MLE**

*4.2.2 Lyapunov Exponents.* Lyapunov exponents provide a quantitative means for indicating the presence of chaos, by providing averaged rates of divergence or convergence of two infinitesimally close trajectories onto an attractor in state space. Since $n$ independent initial vectors in $n$-dimensional space are tested to calculate the rate of the separation, there is a spectrum of LEs. The maximum value of the Lyapunov exponent (MLE) is an important indicator to determine chaos of local responses. A positive value of the MLE indicates chaotic behavior and a negative indicates an absence of chaos.

*4.2.3 Path to Chaos.* There are several routes to chaos of dynamic systems. The period doubling path is a succession of period doublings events as a control parameter is monotonically increased leading to a state of chaos. Another path to chaos is intermittency, which refers to the abrupt transition of a periodic response to chaos due to outbreaks or bursts of NL effects at irregular intervals. A quasiperiodic path to chaos occurs due to the breaking or doubling oscillations, which is a result of a series of Hopf and secondary Hopf bifurcations. Sundararajan and Noah [23] identified a period doubling path to chaos in a journal bearing-supported rotor system. Kim and Palazzolo [35] found intermittency and quasiperiodic paths to chaos in the simulation of a rigid rotor-floating ring bearing system. Chu and Zhang [106] examined the periodic doubling and intermittency routes to chaos in a rub-impact Jeffcott rotor-bearing system.

## 5 Examples

Kim and Palazzolo's prior work [35–37,85] illustrates NL responses in rotordynamic systems with full floating ring bearings or tilting pad journal bearings. These cases show distinctly nonlinear behaviors, including coexistent solutions, bifurcations, and chaos, and were analyzed with the numerical techniques previously described, i.e., the shooting and continuation algorithms, Lyapunov exponents, Poincaré maps, transient numerical integration, etc.

**5.1 Floating Ring Bearings System.** Floating bushing bearings, also called FRBs, are a special type of journal bearing with double layered lubricant films on the inner and the outer surfaces. Although FRBs have strong nonlinearity and are a source of instability, due to their high functionality and cost-effective performance, they are widely used for automotive turbochargers and other high-speed lightly loaded applications.

*5.1.1 Nonlinear Response and Chaos.* In general, FRBs operate at very high speeds, e.g., 150 k–350 krpm, and normally exhibit steady-state NL response [35]. In the present study [107], a symmetric rigid rotor supported on FRBs is simulated using the improved numerical shooting and continuation algorithms, along with standard TNI. Deflation and parallel computing are implemented due to the large order of the finite element model. Figure 6 shows three coexisting, sub-synchronous responses at 80,000 rpm, as obtained by applying the shooting method. These

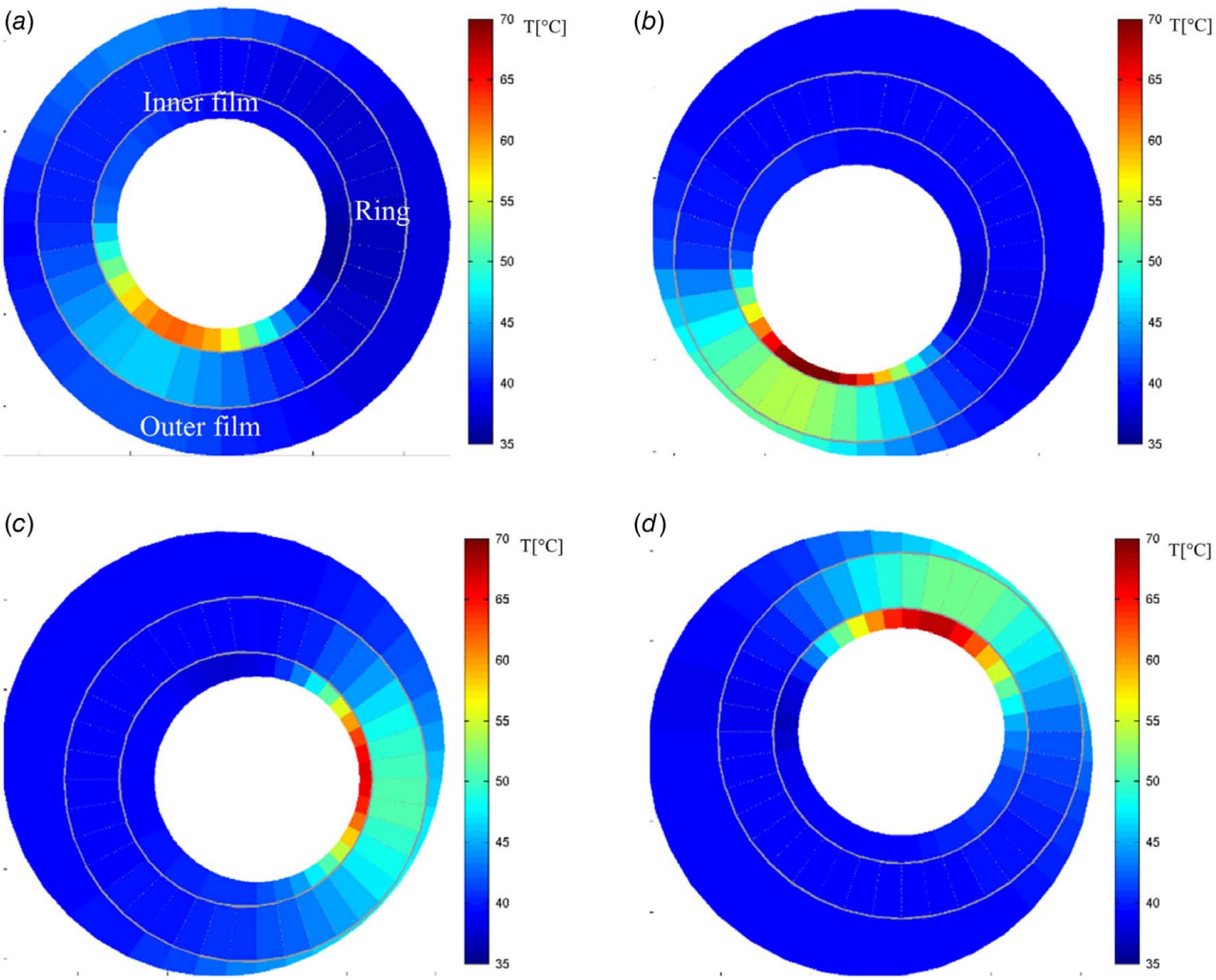


**Fig. 11 FRB temperature distributions at specific times, utilizing the THD shooting method**

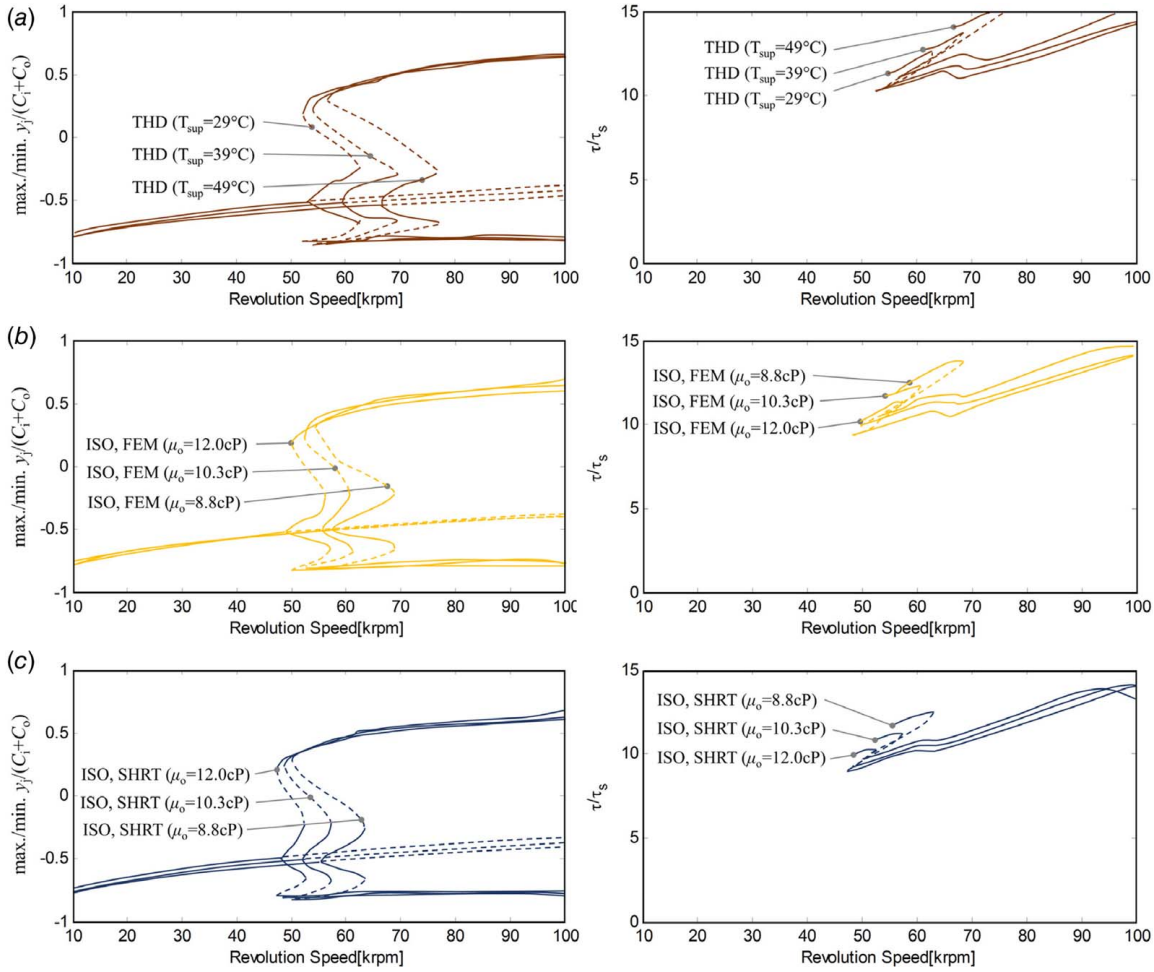


**Fig. 12 Comparison of bifurcation diagrams for (*a*) THD finite lubricant model, (*b*) isothermal-finite lubricant model, and (*c*) isothermal-short bearing approximation model**

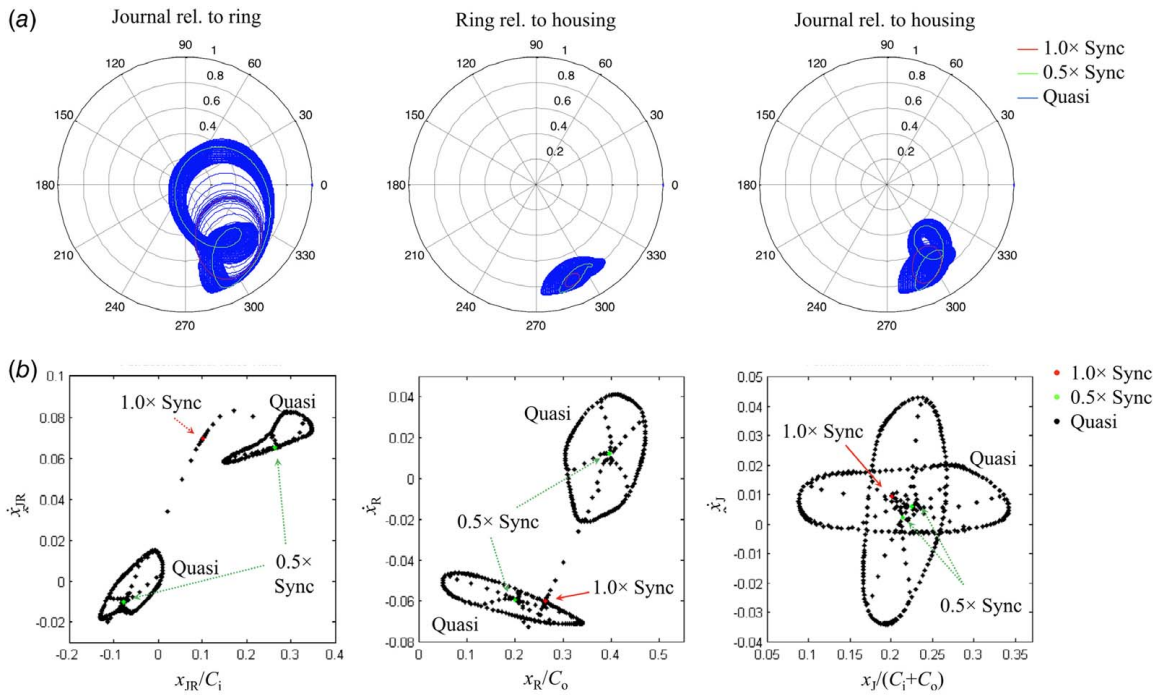


**Fig. 13 Repelling motion from 1× synchronous to quasiperiodic response at 22,000 rpm ($\epsilon = 0.3$, $T_{supply} = 39$ °C): (*a*) orbits at relative position and (*b*) corresponding Poincaré sections**

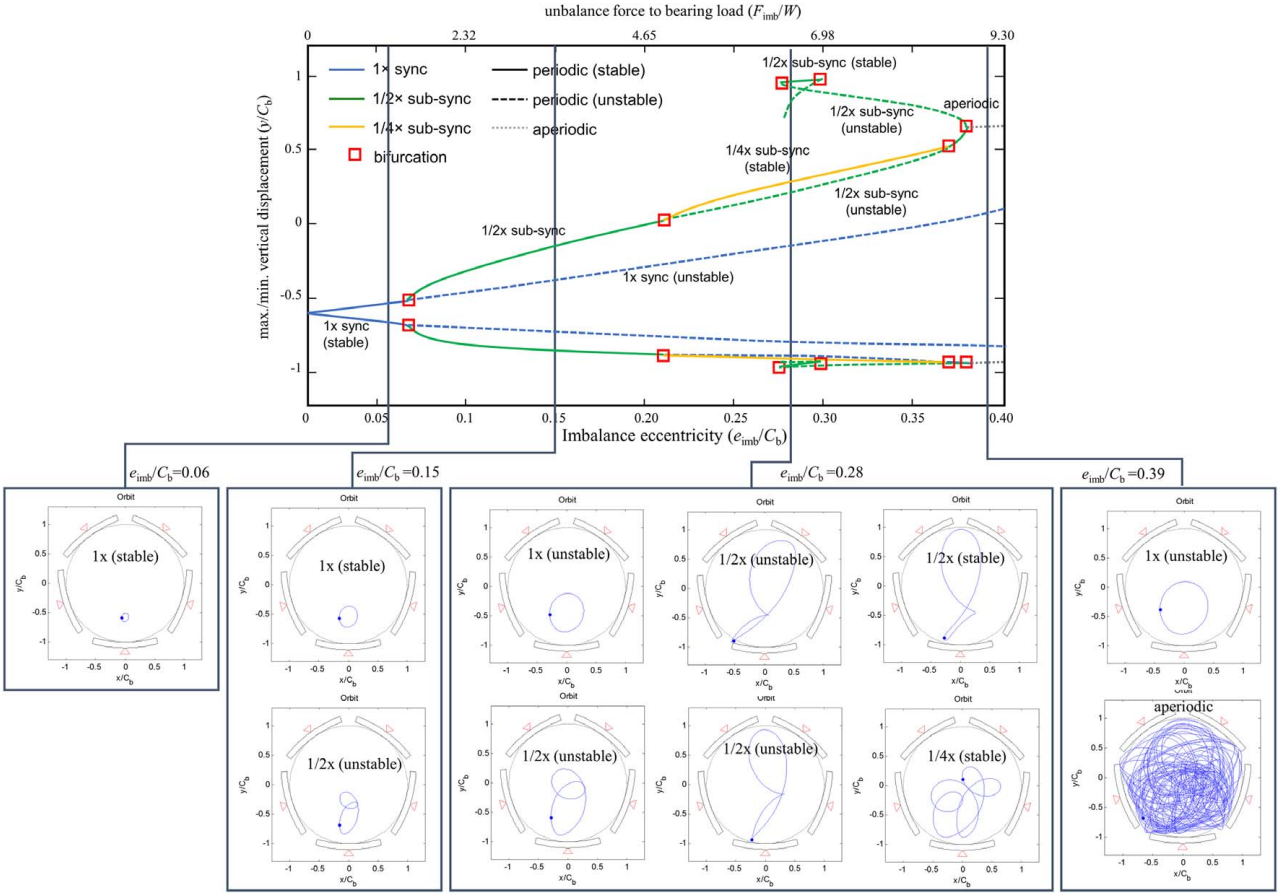


**Fig. 14 Bifurcation diagram and coexisting solutions using shooting/continuation with respect to imbalance eccentricity on disk (rpm = 16,000, $m_p = 1/2$, $\alpha/\beta = 0.5$, and $\mu = 13.8$ mPa·s)**

include two stable and one unstable limit cycle. The potential danger of coexisting stable limit cycles is that the response could jump out of the domain of attraction (DOA) of a benign limit cycle into the DOA of a destructive one, following a sufficient disturbance. Figure 7(*a*) shows such an instance following an impulse loading applied to the support of the rotor. Arc-length continuation provides an economical means to extend the plot of the response versus some system parameter such as rotor speed, as illustrated in Fig. 8. This shows both nondimensional motion and period variable plots versus rpm. The latter response variable results from the model having zero external force (imbalance, $\epsilon = 0.0$), thus no excitation period. The limit cycle period is made nondimensional $\tau/\tau_s$, with respect to the rotation period $\tau_s$ where $\tau_s$ is the spinning period $2\pi$. An imbalance, $\epsilon = 0.4$, is mounted on the disk for the nonautonomous case.

Poincaré sections and the corresponding maximum Lyapunov exponent are plotted versus rpm from 5000 rpm to 50,000 rpm in Fig. 9. Various response states, including ×1 synchronous, ×1/3 sub-synchronous, quasiperiodic, and aperiodic motions are identified. The MLE distinguishes chaotic motions from the quasiperiodic responses, and the MLE diagram implies chaos #1 emerges from a quasiperiodic route to chaos, and chaos #2 emerges from an intermittency route.

Figure 10 examines dynamic status at the operation condition, 20,000 rpm, from the bifurcation diagram. The orbits and ring speed obviously aperiodic and the Poincaré maps are not typical

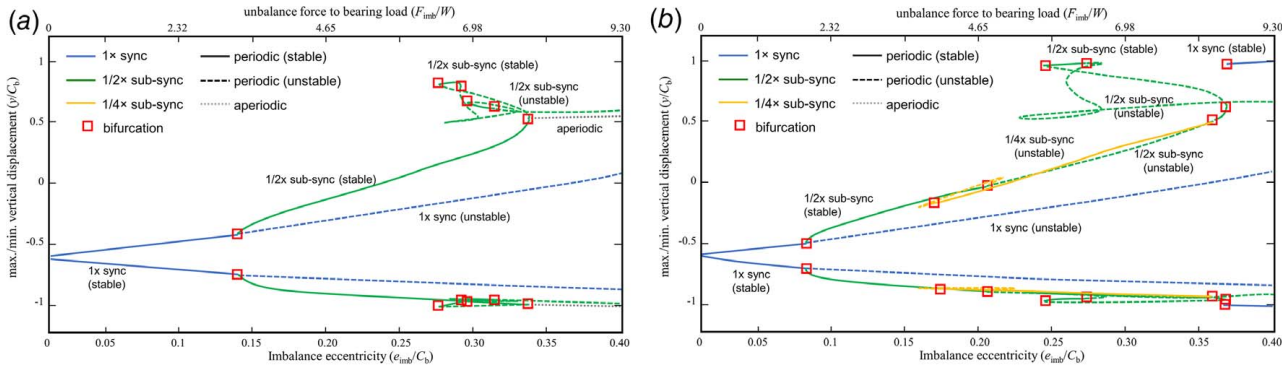


**Fig. 15 Bifurcation diagrams with respect to pad preloads ($m_p$) and pivot offset ($\alpha/\beta$): (*a*) $m_p = 1/2$ and $\alpha/\beta = 0.6$ and (*b*) $m_p = 2/3$ and $\alpha/\beta = 0.5$**

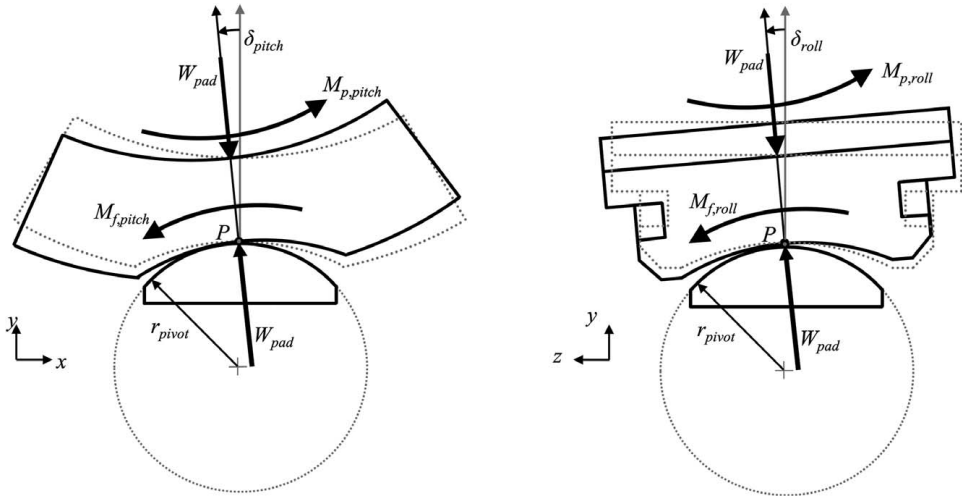


**Fig. 16 Pad-pivot friction mechanism in a spherical pivot type TPJB**

patterns like a point or closed curves but peculiar such as humming birds or flowers. The frequency spectrum has the broad and irregular components along the domain. The spectrum of LEs and MLE have role to quantitatively decide whether the motion is chaos or not; here, MLE remains in the positive value. All of these evaluations confirm the response is chaos.

*5.1.2 Thermal-Hydrodynamic Nonlinear Effect on Rotordynamic Bifurcation.* The previous study assumes an isothermal lubricant condition. The study [36] included THD effects in the bifurcation study. The shooting and continuation algorithms include an additional solution routine to solve the energy equation and the variable viscosity Reynolds equation simultaneously. This provides a thermo-hydrodynamic based pressure distribution in the lubricant film. The integrated pressure forces are transferred into the rotor governing equations during the shooting and arc-length continuation-based solution procedure. The computational task is accelerated by using efficient numerical approaches, including deflation and parallel computing.

Thermo-hydrodynamic shooting can simultaneously identify multiple coexisting solutions that maintain equilibria of orbital and thermal states under identical operating conditions. Figure 11 represents the temperature distributions over a cross-sectional plane of the FRB at specific time instants for an identified limit cycle. Figures

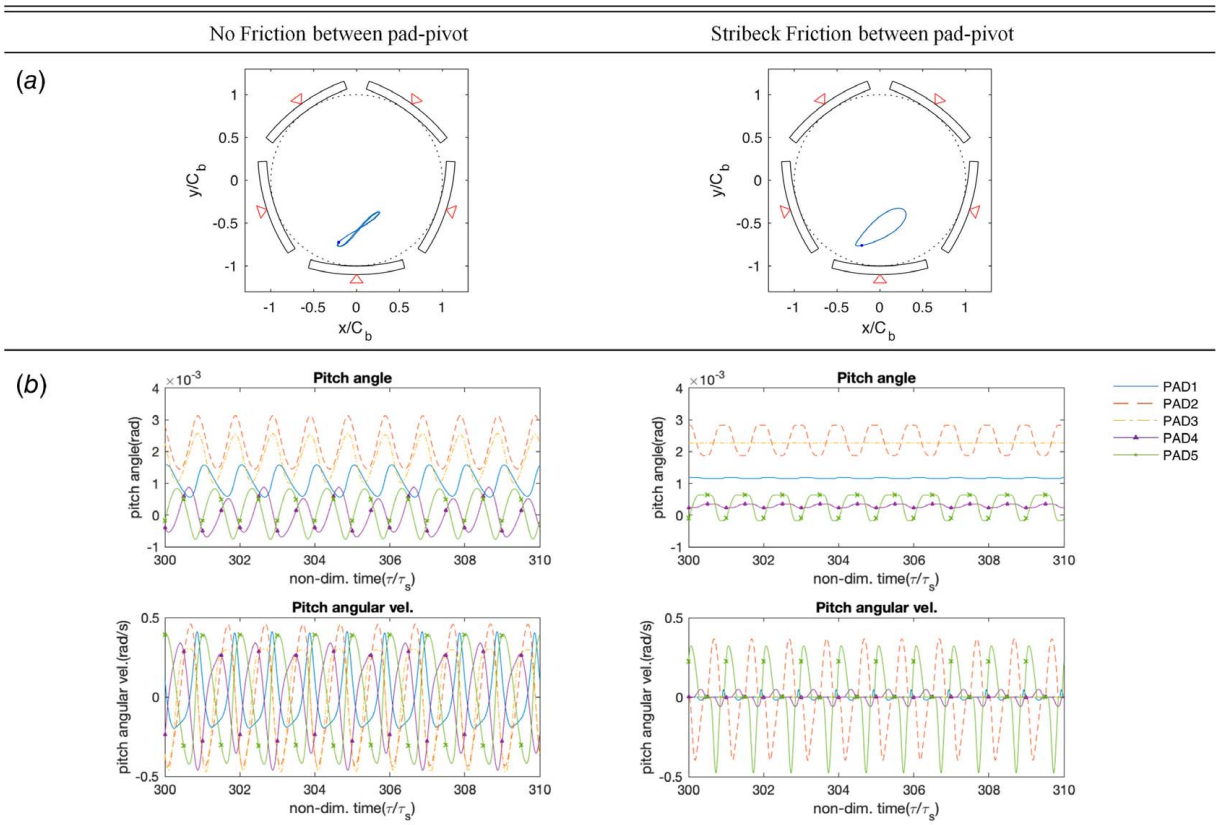


**Fig. 17 Comparisons of (*a*) journal locus and (*b*) corresponding pad motions for the operation conditions: 5000 rpm, $e_{imb} = 0.2C_b$, and with/without pad-pivot friction**

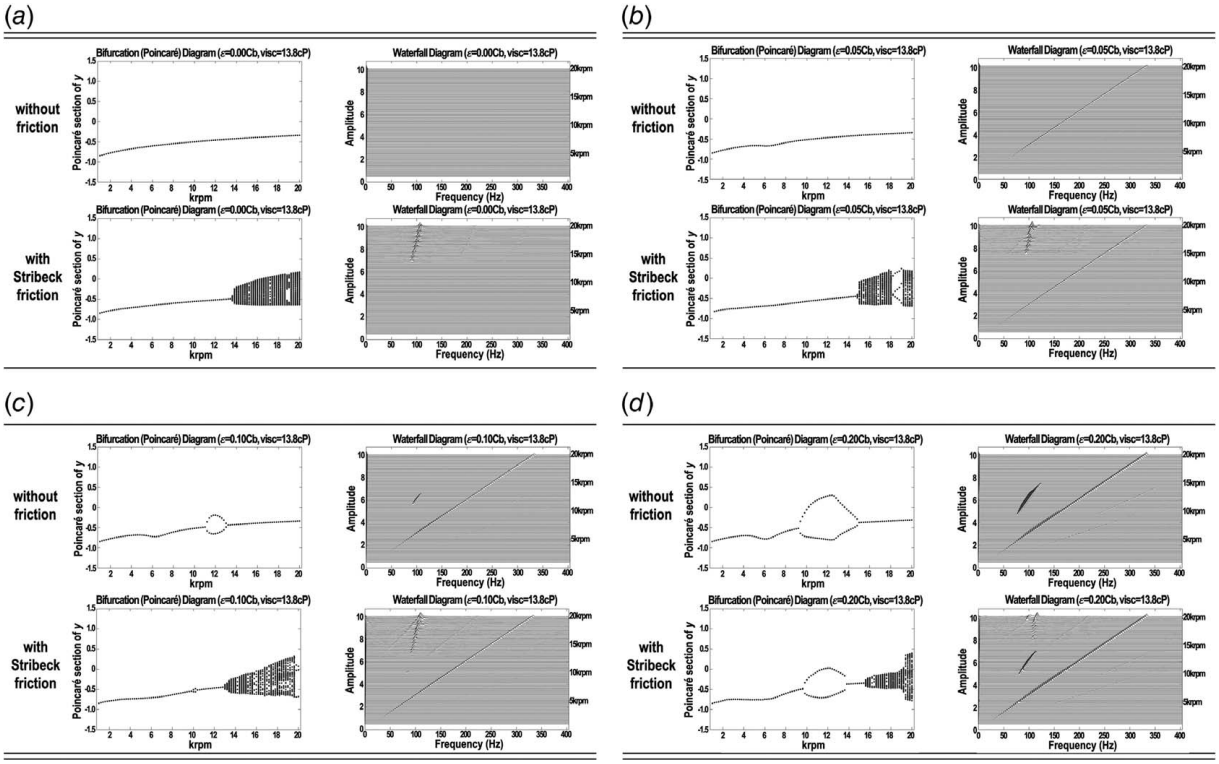


**Fig. 18 Bifurcation diagrams and related waterfall diagrams with/without friction between pad and pivot: (*a*) $e_{imb} = 0$, (*b*) $e_{imb} = 0.05C_b$, (c) $e_{imb} = 0.10C_b$, and (*d*) $e_{imb} = 0.20C_b$**

12(*a*)–12(*c*) compare bifurcation diagrams for different levels of lubricant modeling sophistication. The results indicate that the Hopf bifurcation onsets and the range between saddle nodes are affected by modeling approach. The more accurate THD model (Fig. 12(*a*)) shows a wider speed range of coexistent solutions, and potential jumps from possibly benign to destructive vibration levels. The THD based, autonomous solutions also exhibit a higher sensitivity to the lubricant supply temperature than the isoviscous model results.

Figure 13 shows the predicted multiple response states when the THD shooting algorithm is applied at 22,000 rpm with $T_{sup} =$ 39 °C. The relative positions of the journal orbits and the corresponding Poincaré sections illustrate the transition of the response state from the 1× synchronous to the 1/2× sub-synchronous, and finally to the quasiperiodic.

**5.2 Tilting Pad Journal Bearing System.** Tilting pad journal bearings are widely used in modern turbomachinery such as gas/steam turbines, generators, compressor, and gearboxes due to their stabilizing effects on the rotor systems. The tilt motions of pads suppress cross coupled stiffness and enhance the stability. However, higher performance and efficiency demands push TPJBs to operate under conditions that induce strong instability and NL responses.

*5.2.1 Nonlinear Response and Bifurcations.* Kim and Palazzolo conducted shooting and continuation-based bifurcations studies of a rigid rotor supported on TPJBs [37]. These provided nonautonomous shooting and arc-length continuation algorithms for TPJB applications. The numerical results showed bifurcations, multiple (coexisting) responses states, and chaos of a TPJB rotodynamic system. Parametric studies were performed with numerical continuation, for analyzing the effects of pad preload, pivot offset, and lubricant viscosity on the nonlinear behaviors of TPJBs. These parameters are often varied by machinery designers to obtain optimal vibration control.

As shown in Fig. 14, small windows in the bifurcation diagram show a rich variety of orbital states at specific sections. All

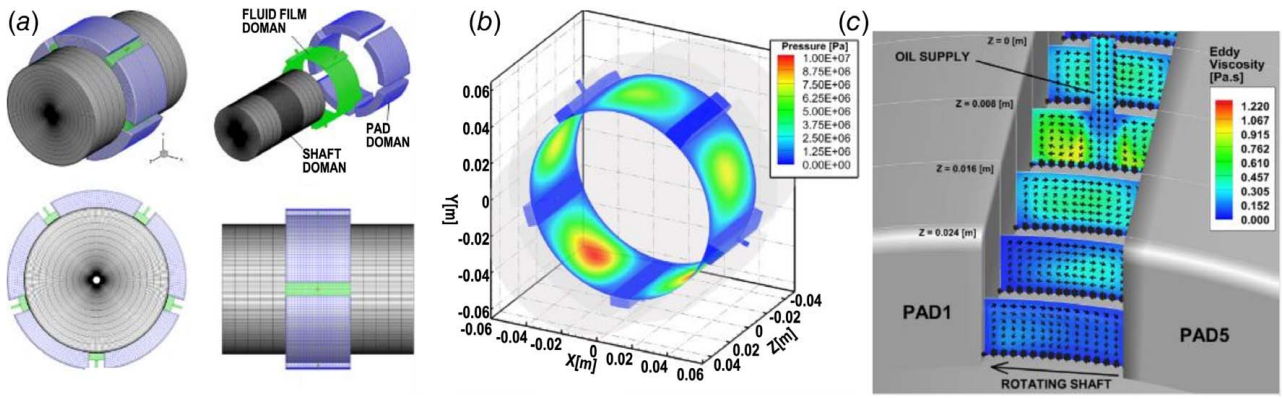


**Fig. 19 CFD based NL bearing model response [109]: (*a*) CFD modeling, (*b*) pressure distribution, and (*c*) oil flow and viscosity**

coexistent solutions are plotted, and the stability of each solution is determined by the Floquet theory.

Figure 15 illustrates the solution branches obtained from shooting/continuation, for two sets of the pad–pivot parameters: pad preload and pivot offset.

*5.2.2 Pad-Pivot Friction Effect on Nonlinear Response.* Friction between TPJB pads and supporting pivots may significantly affect rotordynamic stability and response [85]. This section considers the effects of pad-pivot friction, represented with a Stribeck friction model, on the response of an autonomous and a nonautonomous rotor system. Specifically, nonlinear behaviors such as subsynchronous limit cycles, quasiperiodic responses, Hopf bifurcation, and Neimark- Sacker bifurcations are presented.

Figure 16 illustrates the pad-pivot friction moments. The friction force impedes the tilting motion of the pad by generating the friction moment, $M_f$, which has different formulas for the sliding/tilting pad case and the stuck pad case. Figure 17 shows that pad-pivot friction causes an increase in the size of the rotor's synchronous 1× response orbit, and a decrease in the pad angle amplitudes.

Figure 18 shows the Poincaré sections and corresponding waterfall diagrams for different imbalance eccentricities, with/without pad-pivot friction. The figure implies that the pad-pivot friction plays a significant role in the non- linear response of the tilting pad journal bearing system, especially under high-speed and high unbalance operations.

## 6 Discussions

The nonlinear elements in a journal bearing affect the rotordynamic performance such as orbit size and minimum film thickness and also exert a significant effect on the onset of nonlinear vibrations including sub-, super-synchronous, quasiperiodic motion, chaos, and thermally induced instabilities. The present paper offers a comprehensive review on types of nonlinear forces and their effect on rotordynamic vibration, as well as modeling and solution approaches for nonlinear response prediction. Examples of characteristic nonlinear responses resulting from nonlinear forces in journal bearings are presented, with various solution approaches. Possible future work includes even higher-fidelity TEHD bearing modeling for more accurate prediction of nonlinear response. Yang and Palazzolo [108,109] first developed a three-dimensional CFD model for a tilting pad journal bearing that includes multiphase flow, thermal-fluid, transitional turbulence, and thermal deformation of the shaft and pads as illustrated in Fig. 19. The CFD approach includes detailed modeling of the thermal-flow mixing of hot and cool lubricants between pads, as opposed to the commonly used mixing coefficient method used with Reynolds models.

Additional work includes improving the computational efficiency of the coupled, FEM, nonlinear bearing—flexible rotor system simulation.


## Acknowledgment

The authors gratefully acknowledge the support of this research from the Texas A&M Turbomachinery Research Consortium and National Research Foundation of Korea (2020R1F1A1071976).


## Conflict of Interest

There are no conflicts of interest.

## Data Availability Statement

The authors attest that all data for this study are included in the paper.

## Nomenclature

$j$ = index
$t$ = time
$D$ = journal diameter
$L$ = bearing length
$T$ = time period
$\mathbf{c}$ = coefficient vector
$\mathbf{C}$ = damping matrix
$\mathbf{F}$ = force vector
$\mathbf{I}$ = identity matrix
$\mathbf{K}$ = stiffness matrix
$\mathbf{M}$ = mass matrix
$e_{imb}$ = imbalance eccentricity
$m_p$ = pad preload
$C_b$ = bearing clearance
$C_p$ = pad clearance
$M_f$ = friction moment
$\mathbf{J}_x$ = Jacobian matrix with respect to state vector $\mathbf{x}$
$\mathbf{J}_\tau$ = Jacobian matrix with respect to time period $\tau$
$\mathbf{a}$, $\mathbf{b}$ = coefficients in trigonometric series
$\mathbf{x}$, $\mathbf{z}$ = state vectors
$\mathbf{A}$, $\mathbf{B}$ = system matrices
$\alpha/\beta$ = pivot offset
$\varepsilon$ = nondimensional imbalance eccentricity ($= e_{imb}/C_b$)
$\mu$ = lubricant viscosity
$\tau$ = nondimensionalized time
$\omega$ = oscillation frequency

## References


[1] Muszynska, A., 1986, "Whirl and Whip—Rotor/Bearing Stability Problems," J. Sound Vib., **110**(3), pp. 443–462.
[2] Muszynska, A., 1988, "Stability of Whirl and Whip in Rotor Bearing System," J. Sound Vib., **127**(1), pp. 49–64.
[3] Schweizer, B., 2009, "Oil Whirl, Oil Whip and Whirl/Whip Synchronization Occurring in Rotor Systems With Full-Floating Ring Bearings," Nonlinear Dyn., **57**(4), pp. 509–532.
[4] De Castro, H. F., Cavalca, K. L., and Nordmann, R., 2008, "Whirl and Whip Instabilities in Rotor-Bearing System Considering a Nonlinear Force," J. Sound Vib., **317**(1-2), pp. 273–293.
[5] San Andres, L., and Kerth, J., 2004, "Thermal Effects on the Performance of Floating Ring Bearings for Turbochargers," Proc. Inst. Mech. Eng. J., **218**(5), pp. 437–450.
[6] Clarke, D. M., Fall, C., Hayden, G. N., and Wilkinson, T. S., 1992, "A Steady-State Model of a Floating Ring Bearing, Including Thermal Effects," ASME J. Tribol., **114**(1), pp. 141–149.
[7] Suh, J., and Palazzolo, A. B., 2015, "Three-Dimensional Thermohydrodynamic Morton Effect Simulation—Part I: Theoretical Model," ASME J. Tribol., **136**(3), p. 031706.
[8] Suh, J., and Palazzolo, A. B., 2015, "Three-Dimensional Dynamic Model of TEHD Tilting-Pad Journal Bearing—Part II: Parametric Studies," ASME J. Tribol., **137**(4), p. 041704.
[9] Reinhardt, E., and Lund, J. W., 1975, "The Influence of Fluid Inertia on the Dynamic Properties of Journal Bearings," ASME J. Lubr. Technol., **97**(2), pp. 159–165.
[10] San Andres, L., 1990, "Turbulent Hybrid Bearings With Fluid Inertia Effects," ASME J. Tribol., **112**(4), pp. 699–707.
[11] Childs, D., 1993, *Turbomachinery Rotordynamics: Phenomena, Modeling, and Analysis*, John Wiley & Sons, New York.
[12] Adiletta, G., Guido, A. R., and Rossi, C., 1996, "Chaotic Motions of a Rigid Rotor in Short Journal Bearings," Nonlinear Dyn., **10**(3), pp. 251–269.
[13] Holt, C., San Andres, L., Sahay, S., Tang, P., La Rue, G., and Gjika, K., 2005, "Test Response and Nonlinear Analysis of a Turbocharger Supported on Floating Ring Bearings," ASME J. Vib. Acoust., **127**(2), pp. 107–115.
[14] Tian, L., Wang, W. J., and Peng, Z. J., 2013, "Nonlinear Effects of Unbalance in the Rotor-Floating Ring Bearing System of Turbochargers," Mech. Syst. Signal Process., **34**(1–2), pp. 298–320.
[15] Tian, L., Wang, W. J., and Peng, Z. J., 2011, "Dynamic Behaviours of a Full Floating Ring Bearing Supported Turbocharger Rotor With Engine Excitation," J. Sound Vib., **330**(20), pp. 4851–4874.
[16] Kim, Y. B., and Noah, S. T., 1990, "Bifurcation Analysis for Modified Jeffcott Rotor With Bearing Clearances," Nonlinear Dyn., **1**(3), pp. 221–241.
[17] Kim, Y. B., and Noah, S. T., 1991, "Periodic Response of Multi-Disk Rotors With Bearing Clearances," J. Sound Vib., **144**(3), pp. 381–395.
[18] Kim, Y. B., and Noah, S. T., 1991, "Response and Bifurcation Analysis of a MDOF Rotor System With a Strong Nonlinearity," Nonlinear Dyn., **2**(3), pp. 215–234.
[19] Kim, Y. B., and Noah, S. T., 1991, "Steady-State Analysis of a Nonlinear Rotor-Housing System," ASME J. Eng. Gas Turbines and Power, **113**(4), pp. 550–556.

[20] Groll, G., and Ewins, D. J., 2001, "The Harmonic Balance With Arc-Length Continuation in Rotor/Stator Contact Problems," J. Sound Vib., **241**(2), pp. 223–233.
[21] Nataraj, C., and Nelson, H. D., 1989, "Periodic Solutions in Rotor Dynamic Systems With Nonlinear Supports: A General Approach," ASME J. Vib. Acoust. Stress Reliab. Des., **111**(2), pp. 187–193.
[22] Jean, A. N., and Nelson, H. D., 1990, "Periodic Response Investigation of Large Order Non-Linear Rotordynamic Systems Using Collocation," J. Sound Vib., **143**(3), pp. 473–489.
[23] Sundararajan, P., and Noah, S. T., 1997, "Dynamics of Forced Nonlinear Systems Using Shooting/Arc-Length Continuation Method-Application to Rotor Systems," ASME J. Vib. Acoust., **119**(1), pp. 9–20.
[24] Sundararajan, P., and Noah, S. T., 1998, "An Algorithm for Response and Stability of Large Order Non-Linear Systems—Application to Rotor Systems," J. Sound Vib., **214**(4), pp. 695–723.
[25] Newkirk, B. L., and Taylor, H. D., 1925, "Shaft Whipping Due to Oil Action in Journal Bearing," Gen. Electr. Rev., **28**(8), pp. 559–568.
[26] Monmousseau, P., Fillon, M., and Frene, J., 1997, "Transient Thermoelastohydrodynamic Study of Tilting-Pad Journal Bearings—Comparison Between Experimental Data and Theoretical Results," ASME J. Tribol., **119**(3), pp. 401–407.
[27] Zhao, J. Y., and Hahn, E. J., 1993, "Subharmonic, Quasi-Periodic and Chaotic Motions of a Rigid Rotor Supported by an Eccentric Squeeze Film Damper," Proc. Inst. Mech. Eng. Part C, **207**(6), pp. 383–392.
[28] Chinta, M., and Palazzolo, A. B., 1998, "Stability and Bifurcation of Rotor Motion in a Magnetic Bearing," J. Sound Vib., **214**(5), pp. 793–803.
[29] Wang, J. K., and Khonsari, M. M., 2005, "Application of Hopf Bifurcation Theory to Rotor-Bearing Systems With Consideration of Turbulent Effects," Tribol. International, **39**, pp. 701–714.
[30] Wang, J. K., and Khonsari, M. M., 2006, "Influence of Inlet Oil Temperature on the Instability Threshold of Rotor-Bearing Systems," ASME J. Tribol., **128**(2), pp. 319–326.
[31] Wang, J. K., and Khonsari, M. M., 2006, "Bifurcation Analysis of a Flexible Rotor Supported by Two Fluid-Film Journal Bearings," ASME J. Trobol., **128**(3), pp. 594–603.
[32] Wang, J. K., and Khonsari, M. M., 2008, "Effects of Oil Inlet Pressure and Inlet Position of Axially Grooved Infinitely Long Journal Bearings. Part I: Analytical Solutions and Static Performance," Tribol. Int., **41**(2), pp. 119–131.
[33] Wang, J. K., and Khonsari, M. M., 2008, "Effects of Oil Inlet Pressure and Inlet Position of Axially Grooved Infinitely Long Journal Bearings. Part II: Nonlinear Instability Analysis," Tribol. Int., **41**(2), pp. 132–140.
[34] Boyaci, A., Hartmut, H., Seemann, W., Proppe, C., and Wauer, J., 2009, "Analytical Bifurcation Analysis of a Rotor Supported by Floating Ring Bearings," Nonlinear Dyn., **57**(4), pp. 497–507.
[35] Kim, S., and Palazzolo, A. B., 2017, "Shooting With Deflation Algorithm-Based Nonlinear Response and Neimark-Sacker Bifurcation and Chaos in Floating Ring Bearing Systems," ASME J. Comput. Nonlinear Dyn., **12**(3), p. 031003.
[36] Kim, S., and Palazzolo, A. B., 2017, "Effects of Thermohydrodynamic (THD) Floating Ring Bearing Model on Rotordynamic Bifurcation," Int. J. Non-Lin. Mech., **95**, pp. 30–41.
[37] Kim, S., and Palazzolo, A. B., 2018, "Bifurcation Analysis of a Rotor Supported by Five-Pad Tilting Pad Journal Bearings Using Numerical Continuation," ASME J. Tribol., **140**(2), p. 021701.
[38] Monmousseau, P., Fillon, M., and Frene, J., 1998, "Transient Thermoelastohydrodynamic Study of Tilting-Pad Journal Bearings—Application to Bearing Seizure," ASME J. Tribol., **120**(2), pp. 319–324.
[39] Kucinschi, B., and Fillon, M., 1999, "An Experimental Study of Transient Thermal Effects in a Plain Journal Bearing," ASME J. Tribol., **121**(2), pp. 327–332.
[40] Deepak, J. C., and Noah, S. T., 1998, "Experimental Verification of Subcritical Whirl Bifurcation of a Rotor Supported on a Fluid Film Bearing," ASME J. Tribol., **120**(3), pp. 605–609.
[41] De Jongh, F. M., and Morton, P. G., 1994, "The Synchronous Instability of a Compressor Rotor Due to Bearing Journal Differential Heating," ASME International Gas Turbine and Aeroengine Congress and Exposition, Hague, The Netherlands, June, p. V005T14A002.
[42] Balbahadur, A. C., 2001, "A Thermoelastohydrodynamic Model of the Morton Effect Operating in Overhung Rotors Supported by Plain or Tilting Pad Journal Bearings," Ph.D. dissertation, Virginia Tech.
[43] Panara, D., Baldassarre, L., Griffin, D., Mattana, A., Panconi, S., and Meli, E., 2015, "Numerical Prediction and Experimental Validation of Rotor Thermal Instability," Proceedings of the 44th Turbomachinery Symposium, Texas A&M, College Station, TX, Turbomachinery Laboratories.
[44] Tong, X., and Palazzolo, A. B., 2018, "Measurement and Prediction of the Journal Circumferential Temperature Distribution for the Rotordynamic Morton Effect," ASME J. Tribol., **140**(3), p. 031702.
[45] Plantegenet, T., Arghir, M., Hassini, M. A., and Jolly, P., 2020, "The Thermal Unbalance Effect Induced by a Journal Bearing in Rigid and Flexible Rotors: Experimental Analysis," Tribol. Trans., **63**(1), pp. 52–67.
[46] Plantegenet, T., Arghir, M., and Jolly, P., 2020, "Experimental Analysis of the Thermal Unbalance Effect of a Flexible Rotor Supported by a Flexure Pivot Tilting Pad Bearing," Mech. Syst. Signal Process., **145**, p. 106.
[47] Mondy, R. E., 2005, "The Diagnosing and Corrective Actions Taken to Reduce the Effects of Steam Whirl in a General Electric D-11 Steam Turbine," International Symposium for Stability Control of Rotating Machinery ISCORMA-3, Cleveland, OH, Sept. 19–23.
[48] Lu, X., Khonsari, M. M., and Gelink, E. R., 2006, "The Stribeck Curve: Experimental Results and Theoretical Prediction," ASME J. Tribol., **128**(4), pp. 789–794.
[49] Chu, F., and Lu, W., 2005, "Experimental Observation of Nonlinear Vibrations in a Rub-Impact Rotor System," J. Sound Vib., **283**(3–5), pp. 621–643.
[50] Wu, Y., Feng, K., Zhang, Y., Liu, W., and Li, W., 2018, "Nonlinear Dynamic Analysis of a Rotor-Bearing System with Porous Tilting Pad Bearing Support," Nonlinear Dyn., **94**(2), pp. 1391–1408.
[51] Ramesh, J., and Majumdar, B. C., 1995, "Stability of Rough Journal Bearings Using Nonlinear Transient Method," ASME J. Tribol., **117**(4), pp. 691–695.
[52] Turaga, R., Sekhar, A. S., and Majumdar, B. C., 2000, "Non-Linear Transient Stability Analysis of a Rigid Rotor Supported on Hydrodynamic Journal Bearings With Rough Surfaces," Tribol. Trans., **43**(3), pp. 447–452.
[53] Lin, J. R., 2007, "Application of the Hopf Bifurcation Theory to Limit Cycle Prediction of Short Journal Bearings with Isotropic Roughness Effects," Proc. Inst. Mech. Eng., Part J: J. Eng. Tribol., **221**(8), pp. 869–879.
[54] Lin, J. R., 2014, "The Influences of Longitudinal Surface Roughness on Sub-Critical and Super-Critical Limit Cycles of Short Journal Bearings," Appl. Math. Model., **38**(1), pp. 392–402.
[55] Tong, X., and Palazzolo, A. B., 2017, "Double Overhung Disk and Parameter Effect on Rotordynamic Synchronous Instability—Morton Effect—Part I: Theory and Modeling Approach," ASME J. Tribol., **139**(1), p. 011705.
[56] Tong, X., and Palazzolo, A. B., 2017, "Double Overhung Disk and Parameter Effect on Rotordynamic Synchronous Instability—Morton Effect—Part II: Occurrence and Prevention," ASME J. Tribol., **139**(1), p. 011706.
[57] Haugaard, A. M., and Santos, I. F., 2010, "Multi-Orifice Active Tilting-Pad Journal Bearings—Harnessing of Synergetic Coupling Effects," Tribol. Int., **43**(8), pp. 1374–1391.
[58] Zhang, C., Jiang, J. X., and Cheng, H. S., 2000, "A Study of Dynamically Loaded Finite Journal Bearings in Mixed Lubrication Using a Transient Thermohydrodynamic Analysis," Tribol. Trans., **43**(3), pp. 459–464.
[59] Zhang, C., and Cheng, H. S., 2000, "Transient Non-Newtonian Thermohydrodynamic Mixed Lubrication of Dynamically Loaded Journal Bearings," ASME J. Tribol., **122**(1), pp. 156–161.
[60] Zhang, C., 2002, "TEHD Behavior of Non-Newtonian Dynamically Loaded Journal Bearings in Mixed Lubrication for Direct Problem," ASME J. Tribol., **124**(1), pp. 178–185.
[61] Tofighi-Niaki, E., Asgharifard-Sharabiani, P., and Ahmadian, H., 2018, "Nonlinear Dynamics of a Flexible Rotor on Tilting Pad Journal Bearings Experiencing Rub–Impact," Nonlinear Dyn., **94**(4), pp. 2937–2956.
[62] Jang, G. H., and Yoon, J. W., 2002, "Nonlinear Dynamic Analysis of a Hydrodynamic Journal Bearing Considering the Effect of a Rotating or Stationary Herringbone Groove," ASME J. Tribol., **124**(2), pp. 297–304.
[63] Wang, C. C., Yau, H. T., Jang, M. J., and Yeh, Y. L., 2007, "Theoretical Analysis of the Non-Linear Behavior of a Flexible Rotor Supported by Herringbone Grooved Gas Journal Bearings," Tribol. Int., **40**(3), pp. 533–541.
[64] Wang, B., Sun, Y., and Ding, Q., 2016, "Dynamic Characteristics of the Herringbone Groove Gas Journal Bearings: Numerical Simulations," Shock Vib., **2016**, p. 8743016.
[65] Sinhasan, R., and Goyal, K. C., 1995, "Transient Response of a Two-Lobe Journal Bearing Lubricated With Non-Newtonian Lubricant," Tribol. Int., **28**(4), pp. 233–239.
[66] Jagadeesha, K. M., Nagaraju, T., Sharma, S. C., and Jain, S. C., 2012, "3D Surface Roughness Effects on Transient Non-Newtonian Response of Dynamically Loaded Journal Bearings," Tribol. Trans., **55**(1), pp. 32–42.
[67] Kushare, P. B., and Sharma, S. C., 2014, "Nonlinear Transient Stability Study of Two Lobe Symmetric Hole Entry Worn Hybrid Journal Bearing Operating With Non-Newtonian Lubricant," Tribol. Int., **69**, pp. 84–101.
[68] Hashimoto, H., Wada, S., and Ito, J. I., 1987, "An Application of Short Bearing Theory to Dynamic Characteristic Problems of Turbulent Journal Bearings," ASME J. Tribol., **109**(2), pp. 307–314.
[69] Okabe, E. P., and Cavalca, K. L., 2009, "Rotordynamic Analysis of Systems With a Non-Linear Model of Tilting Pad Bearings Including Turbulence Effects," Nonlinear Dyn., **57**(4), pp. 481–495.
[70] Paranjpe, R. S., and Han, T., 1995, "A Transient Thermohydrodynamic Analysis Including Mass Conserving Cavitation for Dynamically Loaded Journal Bearings," ASME J. Tribol., **117**(3), pp. 369–378.
[71] Paranjpe, R. S., 1996, "A Study of Dynamically Loaded Engine Bearings Using a Transient Thermohydrodynamic Analysis," Tribol. Trans., **39**(3), pp. 636–644.
[72] Fatu, A., Hajjam, M., and Bonneau, D., 2006, "A New Model of Thermoelastohydrodynamic Lubrication in Dynamically Loaded Journal Bearings," ASME J. Tribol., **128**(1), pp. 85–95.
[73] Kim, B. J., and Kim, K. W., 2001, "Thermo-Elastohydrodynamic Analysis of Connecting Rod Bearing in Internal Combustion Engine," ASME J. Tribol., **123**(3), pp. 444–454.
[74] Piffeteau, S., Souchet, D., and Bonneau, D., 2000, "Influence of Thermal and Elastic Deformations on Connecting-Rod Big End Bearing Lubrication Under Dynamic Loading," ASME J. Tribol., **122**(1), pp. 181–191.
[75] Childs, D. W., and Saha, R., 2012, "A New, Iterative, Synchronous-Response Algorithm for Analyzing the Morton Effect," ASME J. Eng. Gas. Turb. Power., **134**(7), p. 072501.
[76] Lee, J. G., and Palazzolo, A. B., 2013, "Morton Effect Cyclic Vibration Amplitude Determination for Tilt Pad Bearing Supported Machinery," ASME J. Tribol., **135**(1), p. 011701.
[77] Tong, X., Palazzolo, A. B., and Suh, J., 2016, "Rotordynamic Morton Effect Simulation With Transient, Thermal Shaft Bow," ASME J. Tribol., **138**(3), p. 031705.

[78] Tong, X., and Palazzolo, A. B., 2018, "Tilting Pad Gas Bearing Induced Thermal Bow-Rotor Instability (Morton Effect)," Tribol. Int., **121**, pp. 269–279.
[79] Monmousseau, P., and Fillon, M., 2000, "Transient Thermoelastohydrodynamic Analysis for Safe Operating Conditions of a Tilting-Pad Journal Bearing During Start-Up," Tribol. Int., **33**(3-4), pp. 225–231.
[80] Gadangi, R. K., and Palazzolo, A. B., 1995, "Transient Analysis of Tilt Pad Journal Bearings Including Effects of Pad Flexibility and Fluid Film Temperature," ASME J. Tribol., **117**(2), pp. 302–307.
[81] Gadangi, R. K., Palazzolo, A. B., and Kim, J., 1996, "Transient Analysis of Plain and Tilt Pad Journal Bearings Including Fluid Film Temperature Effects," ASME J. Tribol., **118**(2), pp. 423–430.
[82] Monmousseau, P., Fillon, M., and Frene, J., 1998, "Transient Thermoelastohydrodynamic Study of Tilting-Pad Journal Bearings Under Dynamic Loading," J. Eng. Gas. Turb. Power., **120**(2), pp. 405–409.
[83] Monmousseau, P., and Fillon, M., 1999, "Frequency Effects on the TEHD Behavior of a Tilting-Pad Journal Bearing Under Dynamic Loading," ASME J. Tribol., **121**(2), pp. 321–326.
[84] Fillon, M., Desbordes, H., Frene, J., and Chan Hew Wai, C., 1996, "A Global Approach of Thermal Effects Including Pad Deformations in Tilting-Pad Journal Bearings Submitted to Unbalance Load," ASME J. Tribol., **118**(1), pp. 169–174.
[85] Kim, S., and Palazzolo, A. B., 2019, "Pad-Pivot Friction Effect on Nonlinear Response of a Rotor Supported by Tilting-Pad Journal Bearings," ASME J. Tribol., **141**(9), p. 091701.
[86] Kucinschi, B. R., Fillon, M., Frene, J., and Pascovici, M. D., 2000, "A Transient Thermoelastohydrodynamic Study of Steadily Loaded Plain Journal Bearings Using Finite Element Method Analysis," ASME J. Tribol., **122**(1), pp. 219–226.
[87] El-Butch, A. M., and Ashour, N. M., 2005, "Transient Analysis of Misaligned Elastic Tilting-Pad Journal Bearing," Tribol. Int., **38**(1), pp. 41–48.
[88] Nilsson, L., 1978, "The Influence of Bearing Flexibility on the Dynamic Performance of Radial Oil Film Bearings," Proc. 5th Leeds-Lyon Sympos. Tribol., **9**(1), pp. 331–319.
[89] Desbordes, H., Fillon, M., Chan Hew Wai, C., and Frene, J., 1994, "Dynamic Analysis of Tilting-Pad Journal Bearing—Influence of Pad Deformations," ASME J. Tribol., **116**(3), pp. 621–627.
[90] Hahn, E. J., and Chen, P. Y. P., 1994, "Harmonic Balance Analysis of General Squeeze Film Damped Multidegree-of-Freedom Rotor Bearing Systems," ASME J. Tribol., **116**(3), pp. 499–507.
[91] Al-shyyab, A., and Kahraman, A., 2005, "Non-Linear Dynamic Analysis of a Multi-Mesh Gear Train Using Mid-Term Harmonic Balance Method: Sub-Harmonic Motions," J. Sound Vib., **279**(2), pp. 417–451.
[92] Al-shyyab, A., and Kahraman, A., 2005, "Non-Linear Dynamic Analysis of a Multi-Mesh Gear Train Using Mid-Term Harmonic Balance Method: Period-One Motions," J. Sound Vib., **284**(2), pp. 151–172.
[93] Samoilenko, A. M., and Ronto, N. I., 1979, *Numerical-Analytic Methods of Investigating Periodic Solutions*, Mir Publishers, Moscow.
[94] Mees, A. I., 1981, *Dynamics of Feedback Systems*, Wiley, New York.
[95] Nayfeh, A. H., and Balachandran, B., 2008, *Applied Nonlinear Dynamics: Analytical, Computational and Experimental Methods*, Wiley, New York.
[96] Brown, K. M., and Gearhart, W. B., 1971, "Deflation Techniques for the Calculation of Further Solutions of a Nonlinear System," Numerische Math., **16**(4), pp. 334–342.
[97] Ojika, T., Satoshi, W., and Taketomo, M., 1983, "Deflation Algorithm for the Multiple Roots of a System of Nonlinear Equations," J. Math. Anal. Appl., **96**(2), pp. 463–479.
[98] Kalantonis, V. S., Perdios, E. A., Perdious, A. E., Ragos, O., and Vrahatis, M. N., 2003, "Deflation Techniques for the Determination of Periodic Solutions of a Certain Period," Astrophys. Space Sci., **288**(4), pp. 489–497.
[99] Kumar, V., 2002, *Introduction to Parallel Computing*, Addison-Wesley Longman Publishing Co., Inc., Boston.
[100] Wang, Z., Jin, X., Zhou, Q., Ai, X., Keer, L. M., and Wang, Q., 2013, "An Efficient Numerical Method With a Parallel Computational Strategy for Solving Arbitrarily Shaped Inclusions in Elastoplastic Contact Problems," ASME J. Tribol., **135**(3), p. 031401.
[101] Chouchane, M., and Amamou, A., 2011, "Bifurcation of Limit Cycles in Fluid Film Bearings," Int. J. Non-Linear Mech., **46**(9), pp. 1258–1264.
[102] Amamou, A., and Chouchane, M., 2014, "Nonlinear Stability Analysis of Long Hydrodynamic Journal Bearings Using Numerical Continuation," Mech. Mach. Theory, **72**, pp. 17–24.
[103] Dhooge, A., Govaerts, W., and Kuznetsov, Y. A., 2003, "MATCONT: A MATLAB Package for Numerical Bifurcation Analysis of ODEs," ACM Trans. Math. Software (TOMS), **29**(2), pp. 141–164.
[104] Dhooge, A., Govaerts, W., Kuznetsov, Y. A., Meijer, H. G. E., and Sautois, B., 2008, "New Features of the Software MatCont for Bifurcation Analysis of Dynamical Systems," Math. Comp. Model. Dyn., **14**(2), pp. 147–175.
[105] Boyaci, A., Seemann, W., and Proppe, C., 2009, "Bifurcation Analysis of a Turbocharger Rotor Supported by Floating Ring Bearings," IUTAM Symposium on Emerging Trends in Rotor Dynamics, New Delhi, India, Mar. 23–26.
[106] Chu, F., and Zhang, Z., 1998, "Bifurcation and Chaos in a Rub-Impact Jeffcott Rotor System," J. Sound Vib., **210**(1), pp. 1–18.
[107] Nguyen-Schäfer, H., 2012, *Rotordynamics of Automotive Turbochargers*, Springer, Berlin.
[108] Yang, J., and Palazzolo, A. B., 2019, "Three-Dimensional Thermo-Elasto-Hydrodynamic Computational Fluid Dynamics Model of a Tilting Pad Journal Bearing—Part I: Static Response," ASME J. Tribol., **141**(6), p. 061702.
[109] Yang, J., and Palazzolo, A. B., 2019, "Three-Dimensional Thermo-Elasto-Hydrodynamic Computational Fluid Dynamics Model of a Tilting Pad Journal Bearing—Part II: Dynamic Response," ASME J. Tribol., **141**(6), p. 061703.